Integrated silicon-on-insulator ring resonators with graphene oxide films for increased thermo-optic performance

David Moss

Integrated silicon-on-insulator ring resonators with graphene oxide films for increased thermo-optic performance

David J. Moss

Optical Sciences Centre, Swinburne University of Technology, Melbourne, 3122, Australia; Email: dmoss@swin.edu.au

Keywords

Integrated photonics, 2D materials, thermo-optics

Abstract

The effective control of heat facilitated by advanced thermo-optic materials plays a crucial role in integrated photonic devices, providing key benefits for their functionality and stable operation. Here, we experimentally demonstrate the enhanced thermo-optic performance of silicon microring resonators (MRRs) by co-integrating them with 2D graphene oxide (GO) films. Precise control over the GO films' thicknesses and sizes is achieved, and we characterize thermo-optic response induced by both environmental temperature changes and coupled input light power for devices with GO films of different thicknesses and degrees of reduction. Experimental results show that the GO-coated MRRs exhibit greater wavelength shifts than uncoated MRRs as the environmental temperature rises, while devices with reduced GO (rGO) exhibit the opposite trend. On the other hand, we demonstrate enhanced optical bistability and optical nonreciprocal transmission induced by input coupled light power in the hybrid MRRs. Our work opens up new opportunities for implementing high-performance thermo-optic devices through the on-chip integration of 2D GO films.

1. Introduction

By utilizing the well-developed complementary metal-oxide-semiconductor (CMOS) fabrication technologies,[1-3] integrated photonic devices benefit from the advantages of electronic integrated circuits with respect to the device footprint, energy consumption, and mass producibility. Further, they offer additional benefits such as large processing bandwidths, strong immunity to electromagnetic interference, and the capability for massively parallel processing.[4-6]

Heat management is essential for optimizing the functionality and stability of integrated photonic devices.[7-9] The thermo-optic response of materials, which arises from thermally induced changes in their refractive index and light absorption,[10, 11] plays an important role for heat management in integrated photonic devices. The efficient control of heat facilitated by advanced thermo-optic materials enables the implementation of high-performance thermal emitters,[12, 13] photovoltaics,[14, 15] mode-locked lasers,[16, 17] optical switches,[18, 19] and sensors.[20, 21]

Over the past decades, significant progress in on-chip integration of advanced thermo-optic materials, such as polymers[22-24] and two-dimensional (2D) materials,[25-27] has opened up new avenues for efficient heat control and manipulation in integrated photonic devices. With high flexibility in changing its properties via various reduction methods as well as a strong capability for large-scale integration,[28-30] 2D graphene oxide (GO) has become a highly promising material for implementing hybrid integrated photonic devices. Previously,[31] we characterized the versatile thermo-optic properties of 2D GO films by integrating them onto silicon nitride microring resonators (MRRs).

In this paper, we integrate 2D GO films onto the more widely used silicon photonic platform and characterize the thermo-optic performance of the hybrid devices. We integrate 2D GO films onto silicon MRRs achieving precise control over their thicknesses and areas. We characterize the thermo-optic response caused by both environmental temperature changes and coupled input light power for the fabricated devices with GO films of different thicknesses and degrees of reduction. Experimental results show that the GO-coated MRRs exhibit more significant resonance wavelength shifts in the response of environmental temperature variations as compared to the uncoated MRRs. In contrast, the devices with reduced GO (rGO) show the opposite trend. We also demonstrate enhanced optical bistability and improved optical nonreciprocal transmission (ONT) in the hybrid MRRs induced by input coupled light power. For optical bistability, the devices with GO and rGO exhibit a broader power range for bistable behavior compared to the uncoated devices. For ONT based on the thermo-optic response of dual MRRs, the device with GO achieves the hightest nonreciprocal extinction ratio (*NER*), and at a much lower input power. These results highlight the strong potential of integrating 2D GO films onto silicon photonic platforms to implement high-performance thermo-optic devices.

2. Device fabrication and material characterization

As an oxidized derivative of graphene, GO consists of a carbon network attached with a range of oxygen functional groups (OFGs), such as hydroxyl, epoxide, carboxylic, and carbonyl groups.[28] **Figure 1a** shows the atomic structures of GO, semi-reduced GO (srGO), and totally reduced GO (trGO), together with corresponding illustrations of

their optical bandgaps. The reduction of GO breaks the chemical bonds between the OFGs and the carbon network, leading to the decrease of sp^3 hybridization domain and increase of the sp^2 hybridization domain. Unlike graphene, which has a fully sp^2 domain and a zero optical bandgap,[32] unreduced GO features a large optical bandgap of ΔE = ~2.1 – 3.6 eV due to the presence of isolated sp^3 domain.[33, 34] This yields both low linear and nonlinear light absorption in the infrared wavelength region. For rGO, there is a gradual decrease in the ΔE as the degree of reduction increases, leading to variations in the material properties such as refractive index, optical absorption, and electrical conductivity.[29] In practice, GO can be reduced by using various methods, such as thermal reduction, chemical reduction, microwave reduction, and photoreduction.[28, 35, 36] For trGO with all the OFGs being removed, the bandgap and material properties closely resemble those of graphene, with only slight difference mainly induced by the defects in the carbon network.

Figure 1b illustrates a schematic of a silicon MRR integrated with a 2D GO film. The cross section of the waveguides forming the MRRs (including both the ring and the bus waveguide) was ~ 550 nm × 220 nm. **Figure 1c** shows a microscopic image of a fabricated device with 3 layers of GO. In our fabrication, the MRRs on a silicon-on-insulator (SOI) chip were patterned by using 248-nm deep ultraviolet lithography, and then formed via an inductively coupled plasma etching process. After this, a 1.5-μm-thick silica upper cladding layer was deposited via plasma-enhanced chemical vapor deposition. Finally, windows were opened on the silica upper cladding, followed by the

coating of 2D GO films onto the silicon MRRs, which allows for the interaction between the GO films and the evanescent field of the silicon waveguide mode.

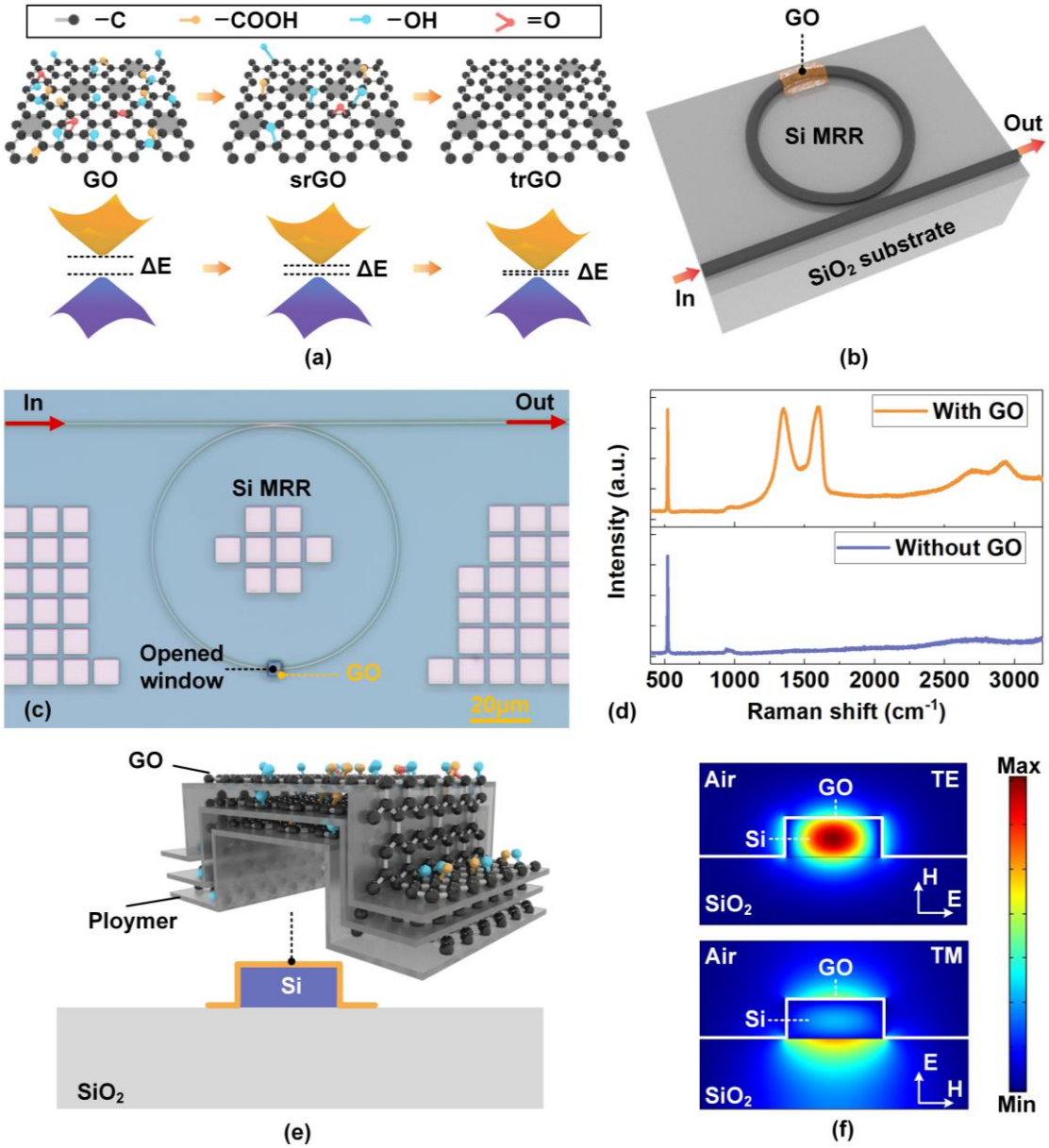

Figure 1. (**a**) Schematic illustration of atomic structures and bandgaps of graphene oxide (GO), semi-reduced GO (srGO), and totally reduced GO (trGO). (**b**) Schematic illustration of a silicon microring resonator (MRR) integrated with a 2D GO film. (**c**) Microscopic image of a fabricated hybrid MRR with 3 layers of GO. (**d**) Measured Raman spectra of a silicon-on-insulator (SOI) chip before and after coating 1 layer of GO. (**e**) Schematic illustration of cross section of the hybrid waveguide with GO. Inset illustrates the layered GO film fabricated by our self-assembly method. (**f**) TE and TM mode profiles for the hybrid waveguide with 3 layers of GO.

Transfer-free and layer-by-layer coating of 2D GO films were achieved by using a solution-based method we developed previously.[37, 38] First, we synthesized negatively charged monolayer GO nanoflakes dispersed in a solution through a modified Hummers method.[29] Next, the fabricated SOI chip with negatively charged surface was immersed in a polymer solution, forming a polymer-coated chip with a positively charged surface. Finally, the chip was immersed in the prepared GO solution with negatively charged 2D GO nanoflakes to complete the coating of 1 layer of GO. By repeating the above processes, a multi-layer film structure consisting of alternating GO monolayers and polymer layers was self-assembled via electrostatic forces. Unlike the film transfer processes employed for other 2D materials such as graphene [39] and transition-metal dichalcogenides (TMDCs),[40] our GO coating approach allows for transfer-free GO film coating on integrated photonic devices as well as precise control over the film thickness. In addition, this method enables conformal coating of 2D GO films onto silicon waveguides with minimal air voids.[41-43] According to atomic force microscope measurements, the thickness of the as-fabricated GO film is ~2 nm / layer.

In **Figure 1c**, the GO film coated on the SOI chip exhibits high transmittance, good morphology, and high uniformity. **Figure 1d** shows the Raman spectra of the same SOI chip before GO and after coating 1 layer of GO, which were measured by using a ~514-nm pump laser. In the measured Raman spectrum for the GO-coated chip, the presence of the featured *D* (~1345 cm^{-1}) and *G* (~1590 cm^{-1}) peaks confirms successful integration of the 2D GO film onto the SOI chip.

Figure 1e illustrates cross section for the hybrid waveguides with 3 layers of GO, with the inset showing a schematic of the layered GO film fabricated by our self-assembly method. **Figure 1f** shows the transverse electric (TE) and the transverse magnetic (TM) mode profiles for the hybrid waveguide with 3 layers of GO, which were simulated via commercial mode-solving software (COMSOL Multiphysics). The corresponding effective refractive indices at 1550 nm were $n_{neff,\,TE}$ = ~2.434 and $n_{neff,\,TM}$ = ~1.629. In our simulation, the refractive indices of GO and silicon at 1550 nm were n_{GO} = 1.984 and $n_{Silicon}$ = 3.445, respectively. These values were obtained from our previous measurements in **Ref.** [31] and the experiments discussed in following sections.

3. Transmission spectra of the hybrid MRRs

After device fabrication, we characterized the transmission spectra of the fabricated MRRs with GO films of varying thicknesses and degrees of reduction. For all the experiments performed in this section, we used silicon MRRs with a radius of ~40 μm, and the length of the opened windows in these MRRs (*i.e.*, the GO film coating length) was ~5 μm. Lensed fibers were employed to achieve light coupling into and out of the fabricated MRRs with inverse-taper couplers at both ends of the bus waveguides. The fiber-to-chip coupling loss was ~5 dB / facet. A polarization controller (PC) was employed to adjust the input light to either TE or TM polarizations when measuring the corresponding transmission spectra.

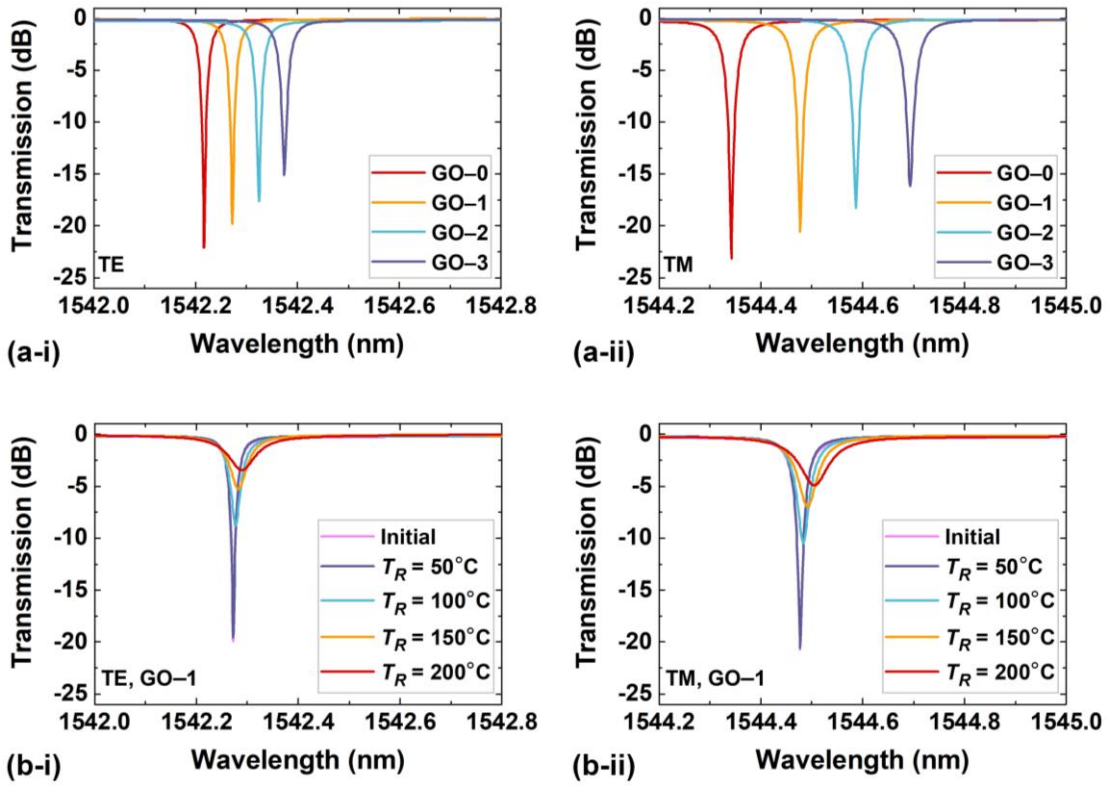

Figure 2. (**a**) Measured (**i**) TE- and (**ii**) TM-polarized transmission spectra of the hybrid MRRs coated with 1−3 layers of GO. The corresponding results for the uncoated silicon MRR (GO-0) are also shown for comparison. (**b**) Measured (**i**) TE- and (**ii**) TM-polarized transmission spectra of a hybrid MRR with 1 layer of GO. The same GO-coated SOI chip was heated on a hot plate for 15 minutes at various temperatures T_R prior to the measurement of its transmission spectra. The corresponding results for the GO-coated SOI chip at room temperature before heating (initial) are also shown for comparison.

Figure 2a compares the measured transmission spectra of the same MRR after coating 1−3 layers of GO. Here we show the results for both TE and TM polarizations, and the corresponding results for the uncoated silicon MRR are also shown for comparison. In order to minimize the wavelength shift induced by thermo-optic effects, we measured all the transmission spectra by scanning the wavelength of an input continuous-wave (CW) light with a power of ~-15 dBm. Unless otherwise specified, the input power in our following discussion represents the value excluding the fiber-to-chip coupling loss. As shown in **Figure 2a**, the MRRs coated with GO films exhibited resonance redshifts compared with the uncoated MRR. As the GO film thickness

increases, the GO-coated MRRs exhibited more significant resonance redshifts. This can be attributed to the change of waveguide effective refractive induced by the coated GO films. Compared to the uncoated silicon MRR, a decrease in the resonance extinction ratios (*ER*s, which refers to the ratio of the maximum to the minimum transmission in the transmission spectra) was observed for the GO-coated MRRs as the GO layer number increases. This is mainly due to the fact that the coated GO films led to an increase in the waveguide propagation loss. By using the scattering matrix method [44, 45] to fit the measured transmission spectra, we obtain that the TE-polarized propagation losses of the uncoated waveguide and the hybrid waveguide with 1 layer of GO are ~4 dB/cm and ~18 dB/cm, respectively. This indicates that the excess propagation loss induced by 1 layer of GO is ~14 dB/cm, which is about two orders of magnitude lower than the reported values for graphene.[46, 47]

Figure 2b shows the measured transmission spectra of a silicon MRR coated with 1 layer of GO for both TE and TM polarizations. We employed a CW light with a power of ~-15 dBm (*i.e.*, the same as that used in **Figure 2a**) to scan the transmission spectra. Before scanning the transmission spectra, the integrated chip was heated on a hot plate for 15 minutes at various temperatures T_R. The measured transmission spectra for the same MRR after heating at different T_R are plotted together with those measured at room temperature prior to heating (labelled as 'initial'). We chose $T_R \leq 200$ °C in our experiments mainly due to the fact that the polymer layers in the self-assembled films cannot withstand temperatures beyond 200 °C.

In **Figure 2b**, there were no significant changes in the transmission spectra of the MRR after heating at T_R = ~50 °C, compared to that measured at room temperature prior to heating. For $T_R \geq$ ~100 °C, the decrease in the *ER* and the redshift of the resonance wavelength reflects that the GO was reduced after the heating process, and rGO exhibits both higher light absorption and refractive index than unreduced GO. A more significant decrease in the *ER* was observed as the degree of reduction increases. This indicates that the changes in the light absorption and refractive index becomes more significant for highly rGO. These results reveal that the coated GO film significantly influences the MRR's transmission spectrum, which can be tailored by controlling the GO film thickness and degree of reduction.

4. Thermo-optic response induced by environmental temperature changes

Thermo-optic effects can arise from variations in environmental temperature, leading to changes in effective refractive indices of optical waveguides and hence resonance wavelength shifts of MRRs. In this section, we characterized the thermo-optic response of hybrid MRRs induced by environmental temperature changes. For the experiments discussed in this section, we employed silicon MRRs with a radius of ~20 μm and with half of each MRR coated by GO films. Compared to those used in **Section 3**, these MRRs can magnify the difference in the measured wavelength shifts caused by GO films. To adjust the temperature of the MRRs, the fabricated chip was placed on a temperature controller with a minimum resolution of ~0.1 °C.

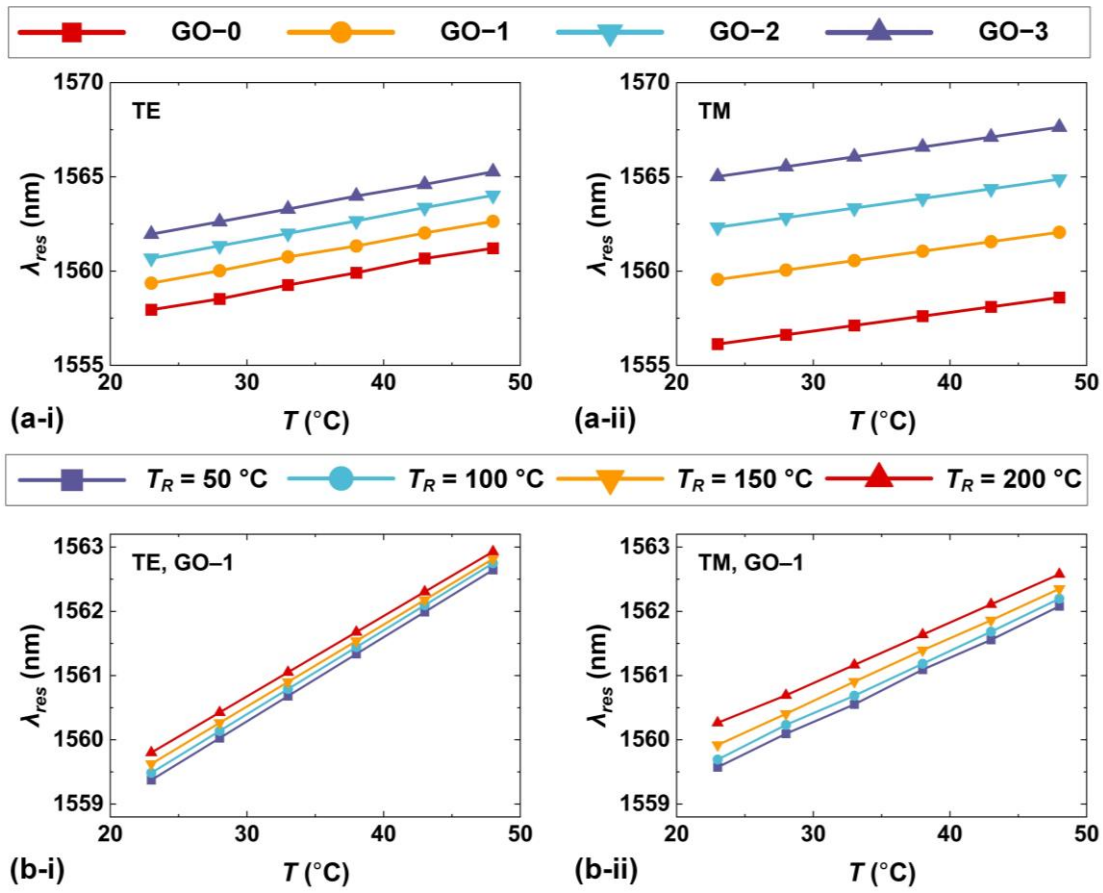

Figure 3. (**a**) Resonance wavelength λ_{res} versus chip temperature T for hybrid MRRs with 1-3 layers of GO. (**i**) and (**ii**) show the results for TE and TM polarizations, respectively. The corresponding results for the uncoated MRR (GO-0) are shown for comparison. (**b**) λ_{res} versus T for a hybrid MRR with 1 layer of GO. The hybrid MRR underwent heating at various temperatures T_R ranging from ~50 to 200 °C prior to the measurement. (**i**) and (**ii**) show the results for TE and TM polarizations, respectively.

Figure 3a shows the measured resonance wavelength λ_{res} as a function of chip temperature T for hybrid MRRs with 1−3 layers of GO. Here we show the results for both TE and TM polarizations, together with the corresponding results for uncoated MRR. To avoid changes in GO film properties induced by thermal reduction, the chip temperature was kept below 50 °C. For all the MRRs, it can be seen that the resonance wavelengths redshifted as the chip temperature increases. Compared to the uncoated MRR that redshifted at a rate of ~130.1 pm/°C for TE polarization, the hybrid MRR with 1 layer of GO exhibited a higher rate of ~130.9 pm/°C, and the rate further

increased to ~132.5 pm/°C for the device with 3 layers of GO. This trend is also observed for TM polarization, with the uncoated MRR and the hybrid MRR with 3 layers of GO redshifting at rates of ~98.4 and ~104.3 pm/°C, respectively. These results indicate that the MRRs exhibited more significant resonance wavelength shifts after integrating 2D GO films. By fitting the measured wavelength shifts with mode simulations, we further extracted the thermo-optic coefficients for 1 layer of GO, which are ~6.5×10^{-4} /°C and ~2.6×10^{-4} /°C for TE and TM polarizations, respectively. These values are higher than that of silicon (*i.e.*, ~1.8×10^{-4} /°C[48]), and show agreement with our previous measurements in Ref. [31]. The difference between the thermo-optic coefficients for TE and TM polarization also reflects the material anisotropy in 2D GO films, which arises from the stronger in-plane light-matter interaction for TE polarization compared to the out-of-plane interaction for TM polarization.[43, 49]

Figure 3b shows the measured λ_{res} versus T for a hybrid MRR with 1 layer of GO after heating at various temperatures T_R. Before measuring λ_{res}, the GO-coated SOI chip was heated on a hot plate at different T_R for 15 minutes (as we did for the experiments in **Figure 2b**). In contrast to the trend observed in **Figure 3a**, the MRRs with rGO (*i.e.*, for $T_R \geq$ 100 °C) exhibited lower rates of resonance wavelength redshift as compared to the uncoated MRR for both TE and TM polarizations. For instance, the device with 1-layer of rGO at T_R = ~200 °C redshifted at a rate of ~125.3 pm/°C for TE polarization, in contrast to ~130.1 pm/°C for the uncoated MRR. These results reflect interesting changes in the thermo-optic response of the hybrid MRRs due to GO reduction, which can be attributed to the fact that rGO at T_R = ~200 °C has a negative thermo-optic

coefficient (*e.g.*, ~-2.5 × 10^{-3} /°C as we measured in Ref. [31]). The decrease in the redshift rates for silicon MRRs with rGO also highlights its potential to mitigate thermal drift caused by temperature fluctuations and enhance the thermal stability of silicon photonic devices.

5. Optical bistability induced by coupled light

In addition to the thermo-optic response caused by environmental temperature changes, high coupled input light intensities can also generate localized temperature variations, leading to changes in the refractive indices of materials. This optically induced thermo-optic response can result in optical bistability phenomena,[50] which are characterized by sharp asymmetric transitional edges and hysteresis loops. By leveraging the transitions between distinct states in the resonator's response to different input power levels, optical bistability can be used for implementing high-performance optical switches, memories, and logic devices.[51-53]

In this section, we investigate optical bistability in hybrid MRRs with 2D GO films. For all the experiments performed in this section, we chose silicon MRR the same as those in **Section 2**, with a radius of ~40 μm, and an opened window length of ~5 μm. The initial wavelength detuning δ in our following discussion was defined as follows:

$$\delta = (\lambda_{laser} - \lambda_{res}) / \Delta\lambda \quad (1)$$

where λ_{laser} is the wavelength of the input CW light, λ_{res} is the resonance wavelength of the MRR measured at a low input power of P_{in} = ~-15 dBm (*i.e.*, the same as that in **Figure 2a**, which does not induce any significant thermo-optic response), and $\Delta\lambda$ is the

resonance 3-dB bandwidth. In our following measurements, we chose the same $\delta = 0.2$ to compare the performance of different devices including an uncoated MRR, hybrid MRRs with 1 and 3 layers of GO, and a hybrid MRR with 1 layer of rGO.

Figures 4a-i and **4a-ii** show the measured output power P_{out} versus input power P_{in} for TE- and TM- polarized resonances of the uncoated silicon MRR, respectively. We first conducted an upward sweeping by slowly increasing P_{in} from ~0.05 mW to ~1.00 mW, and then a downward sweeping with a gradual decrease of P_{in} back within the same power range. For both TE and TM polarizations, in the upward sweeping, there was a gradual increase in the output power as the input power increased, before a sudden drop toward a lower output power. On the other hand, the output power first decreased during the downward sweeping, followed by a sudden jump toward a higher output power. Consequently, hysteresis loops are observed in these figures, serving as a key characteristic of optical bistability and confirming its presence. The power thresholds for the jumps during the upward and downward sweeping are denoted as P_{thes1} and P_{thes2}, respectively.

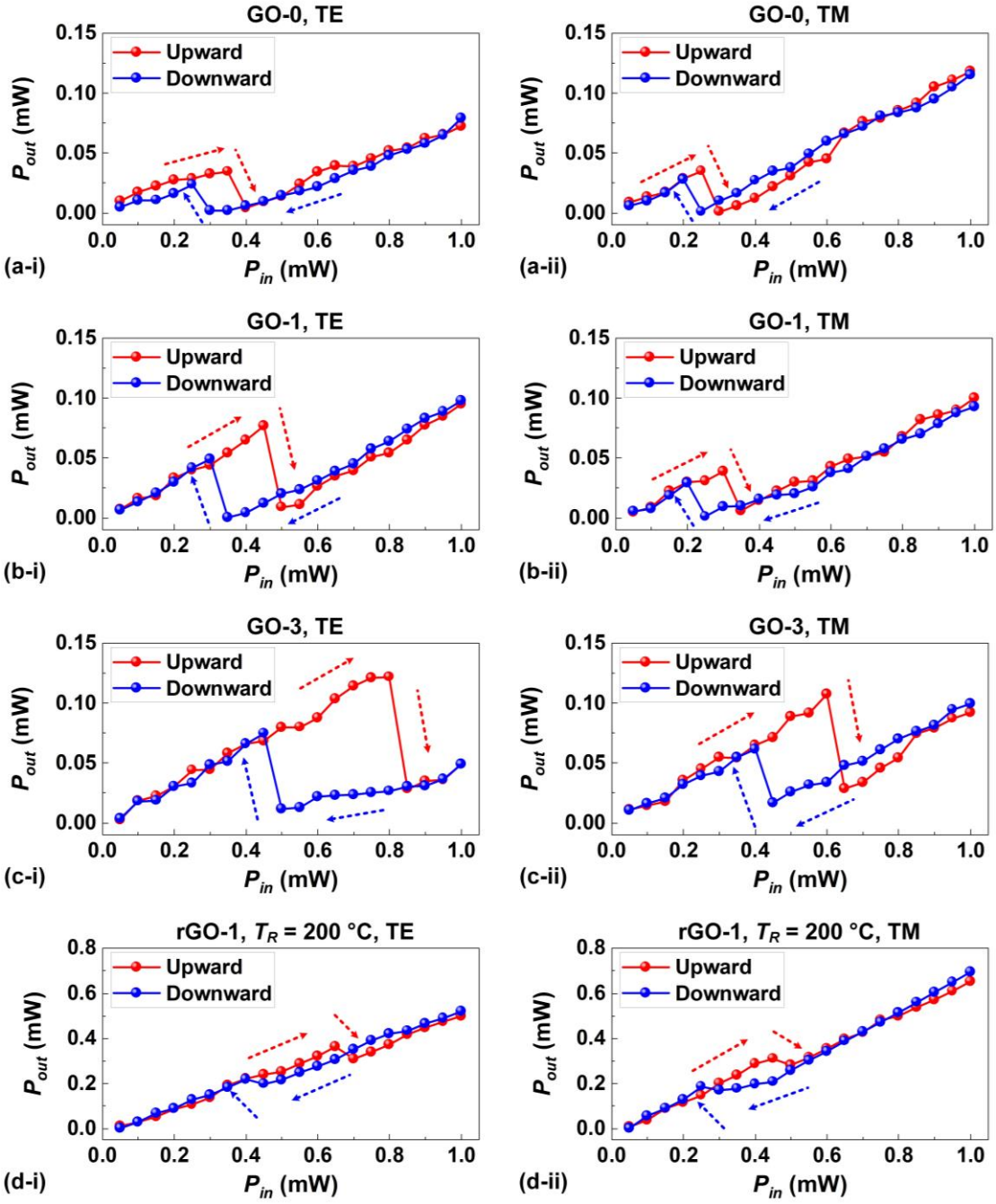

Figure 4. (**a**) Measured output power P_{out} versus input CW power P_{in} for (**i**) TE- and (**ii**) TM-polarized resonances of an uncoated silicon MRR (GO-0), respectively. (**b**) Measured P_{out} versus P_{in} for (**i**) TE- and (**ii**) TM-polarized resonances of a hybrid MRR with 1 layer of GO (GO-1), respectively. (**c**) Measured P_{out} versus P_{in} for (**i**) TE- and (**ii**) TM-polarized resonances of a hybrid MRR with 3 layers of GO (GO-3), respectively. (**d**) Measured P_{out} versus P_{in} for (**i**) TE- and (**ii**) TM-polarized resonances of a hybrid MRR with 1 layer of rGO after heating the chip at T_R = ~200 °C, respectively. In (**a**) – (**f**), the red and blue arrows indicate the increasing and decreasing of the input power, respectively. The initial wavelength detuning was δ = 0.2.

Figures 4b and **4c** show the corresponding results for the hybrid MRRs with 1 and 3 layers of GO, respectively. We carried out the same sweeping processes as those for the measurements in **Figure 4a**. Compared to the uncoated MRR, the MRR with 1 layer of GO showed a larger power range between P_{thes1} and P_{thes2}, and the power range becomes even larger for the device with 3 layers of GO. This indicates that there was enhanced optical bistability in the GO-coated MRRs arising from more significant thermo-optic effects in the GO films. Compared to the TM-polarized resonance, the TE-polarized resonance exhibited a larger power range between P_{thes1} and P_{thes2}. This reflects a more significant thermo-optic response for TE polarization driven by its in-plane light-matter interaction, which is much stronger than the out-of-plane interaction for TM polarization.[42, 43] This result also shows agreement with the relatively large redshift of the resonance wavelength for TE polarization in **Figure 3**.

Figure 4d shows the corresponding results for a hybrid MRR with 1 layer of rGO after heating at T_R = ~200 °C. The device with rGO exhibited a larger power range between P_{thes1} and P_{thes2} as well as smaller power jumps within the hysteresis loop than the comparable device with GO in **Figure 4b**. The former suggests stronger optically induced thermo-optic response in rGO, and the latter mainly results from the decreased *ER* for the device with rGO, as confirmed by the results in **Figure 2b**.

6. Optical nonreciprocal transmission induced by localized light powers

The thermo-optic response can also be harnessed to realize ONT, where light traveling in opposite directions experiences different levels of loss. ONT is of fundamental importance for photonic integrated circuits and forms the basis for optical

diodes and isolators.[54, 55] In this section, we characterize ONT in hybrid MRRs with 2D GO films. In our experiments, we used a fabricated device consisting of dual MRRs, each with a radius of ~20 μm and an opened window length of ~10 μm.

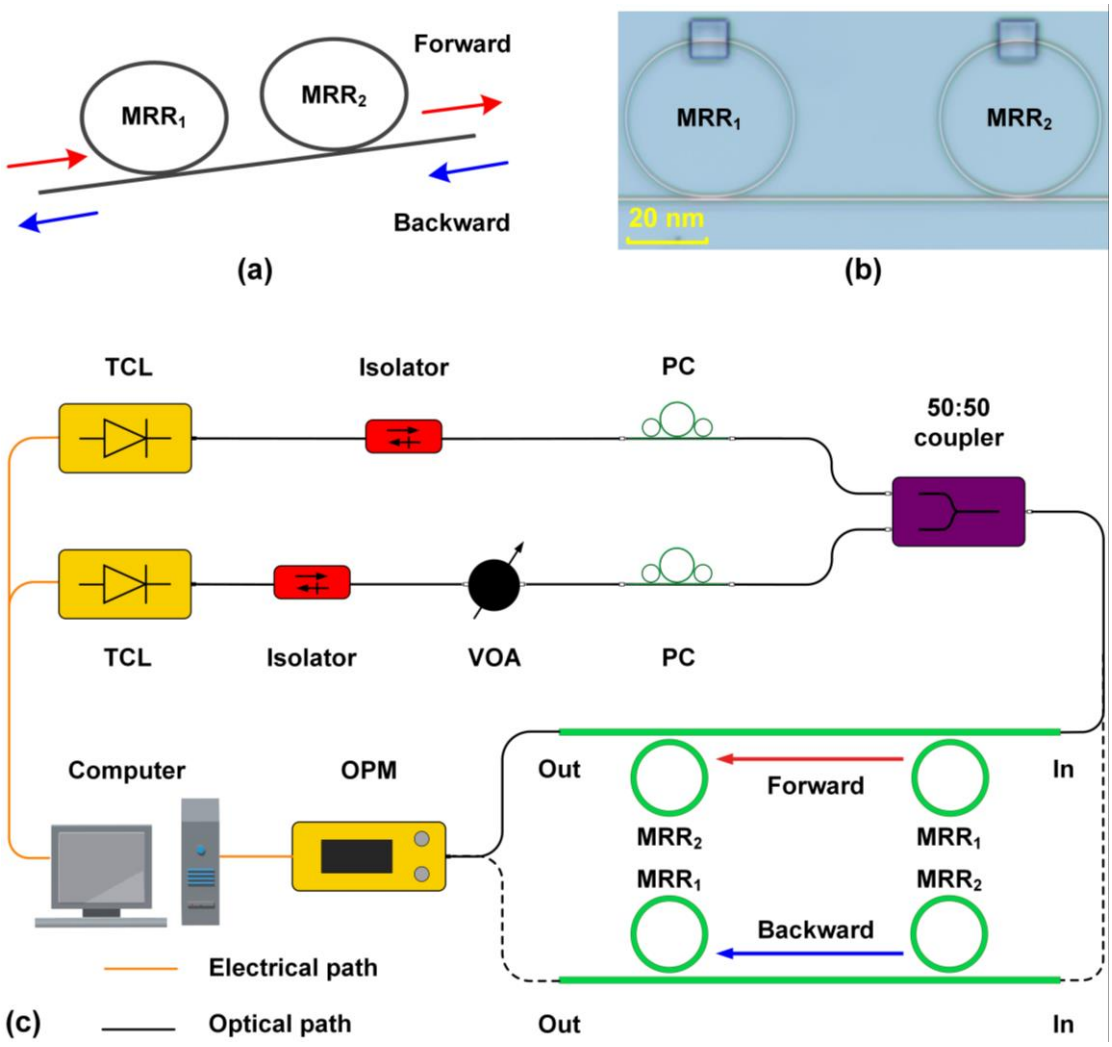

Figure 5. (**a**) Schematic of dual MRRs with forward and backward light propagation. (**b**) Microscopic image of a fabricated device with 1 layer of GO. (**c**) Experimental setup for measuring ONT in the fabricated devices. TCL: tunable continuous-wave laser; VOA: variable optical attenuator; PC: polarization controller. In (**a**) and (**c**), the red and blue arrows indicate the directions for forward and backward propagation, respectively.

Figure 5a shows a schematic of dual MRRs with forward and backward light propagation. For forward transmission, the input light first goes through MRR_1 and then

MRR_2, whereas for backward transmission, the input light passes through MRR_2 first and then MRR_1. A microscopic image of the fabricated device coated with 1 layer of GO is provided in **Figure 5b**.

Figure 5c shows the experimental setup for measuring ONT using the fabricated device in **Figure 5b**. Previously, similar experimental setups were used for measuring ONT in silicon MRRs.[56] In our experiments, two CW lights generated from tunable lasers were employed. The first one, with a power of P_{in} and a wavelength of λ_{in}, served as a high-power input. The second CW light with a low input power of ~-15 dBm (*i.e.*, the same as that in **Figure 2a**, achieved by using a variable optical attenuator (VOA)) was used to scan and characterize the transmission spectrum. These two CW lights were coupled by a 50:50 fiber coupler before being sent to the device under text. The output signal was recorded by an optical power meter (OPM), which was synchronized with the scanning tunable CW laser. Two PCs were used to adjust the two CW lights to TE polarization, and two isolators were employed to protect the lasers from back reflection.

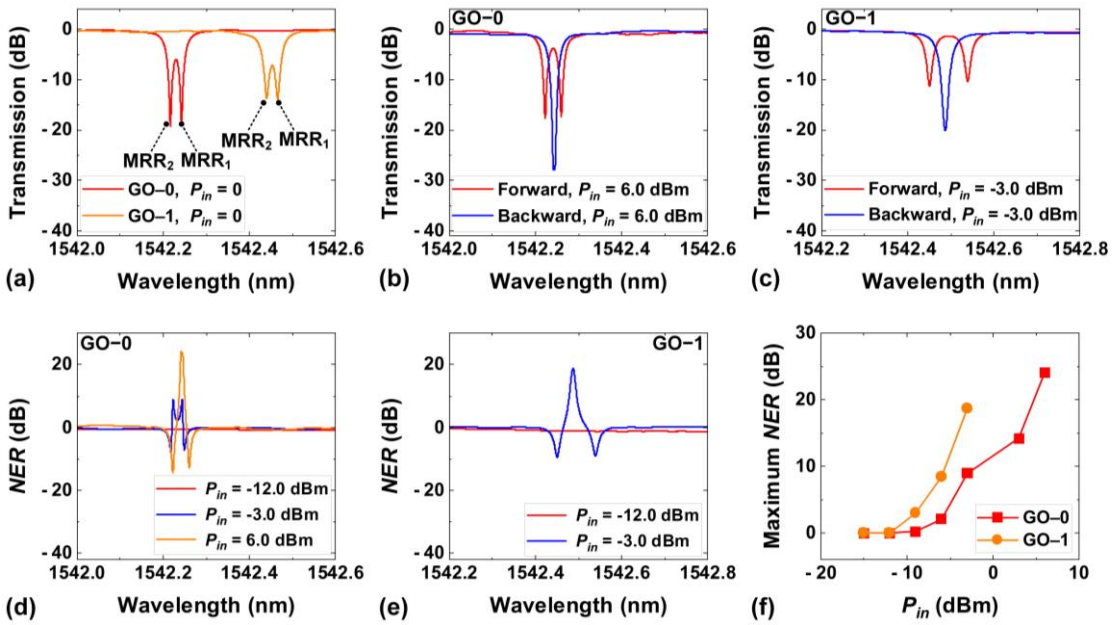

Figure 6. (**a**) Measured transmission spectra of the uncoated dual MRRs (GO-0) and the same device after coating 1 layer of GO (GO-1). (**b**) Measured forward / backward transmission spectra for GO-0 at an input power of P_{in} = ~6.0 dBm. (**c**) Measured forward / backward transmission spectra for GO-1 at P_{in} = ~-3.0 dBm. (**d**) – (**e**) Nonreciprocal extinction ratio (*NER*) at various P_{in} for GO-0 and GO-1, respectively. (**f**) Maximum *NER* versus P_{in} for GO-0 and GO-1.

Figure 6a shows the transmission spectra of the uncoated dual MRRs and the same device after coating 1 layer of GO. These spectra were measured by tuning off the first CW light (*i.e.,* at P_{in} = 0). Due to fabrication errors, the two MRRs with the same designed structural parameters had slightly different resonance wavelengths. For the uncoated MRRs, the resonance wavelengths of MRR_1 and MRR_2 were ~1542.242 nm and ~1542.216 nm, respectively. After coating 1 layer of GO, these two resonance wavelengths shifted to ~1542.466 nm and ~1542.440 nm, respectively. After coating GO, the extinction coefficient of the MRRs became lower, due to a combined result of both the higher propagation loss of GO-coated waveguides and the under-coupled state of the MRRs.[44, 57]

Figure 6b shows the forward and backward transmission spectra of the uncoated dual MRRs (GO-0), which were measured by tuning on the first CW light and slightly tuning its wavelength λ_{in} around the centre between the resonance wavelengths of MRR_1 and MRR_2. Note that in our experiments λ_{in} was tuned around resonances different from those depicted in **Figure 6a**, resulting in the absence of the input CW light in the measured spectra. We tuned λ_{in} from blue to red until the maximum difference between the forward and backward transmission spectra was achieved.

For forward transmission, the resonance wavelength of MRR_1 redshifted from ~1542.242 nm to ~1542.260 nm at P_{in} = ~6.0 dBm and λ_{in} = ~1550.072 nm. In contrast,

no significant redshift was observed for the resonance wavelength of MRR_2, resulting in an increased gap between the resonance wavelengths of MRR_1 and MRR_2. This is because, after passing through MRR_1, the light power was attenuated and insufficient to induce any significant thermo-optic redshifts in MRR_2. For backward light propagation, the resonance wavelength of MRR_2 redshifted from ~1542.216 nm to ~1542.244 nm at the same P_{in} and λ_{in}, whereas the resonance wavelength of MRR_1 did not exhibit significant changes. Consequently, the gap between the resonance wavelengths of MRR_1 and MRR_2 decreased, and the resonances from the two resonators merged into a single one.

In **Figure 6b**, the difference between the forward and backward transmission spectra confirms the presence of ONT in the dual MRRs. Here we select P_{in} = ~6.0 dBm because, at this power, the resonances from the two MRRs nearly merged into a single one, leading to the highest nonreciprocal extinction ratio (*NER*), defined as the maximum difference between the forward and backward transmission spectra.

Figure 6c shows the forward and backward transmission spectra of the dual MRRs in **Figure 6b** after coating with 1 layer of GO (GO-1), which were measured using the same method as that for **Figure 6b**. Similarly, ONT phenomenon was observed for the GO-coated device, and the maximum *NER* was achieved at a much lower input power of P_{in} = ~-3.0 dBm. This highlights the benefits of introducing 2D GO films to reduce the power threshold of photo-thermal effects. It is also worth noting that the maximum *NER* value for the GO-coated device (*i.e.*, ~18.7 dB) is lower than that for the uncoated device (*i.e.*, ~24.0 dB). This is mainly caused by the lower *ER*s of the GO-coated MRRs,

as we discussed in **Figure 6a**. By replacing the under-coupled MRRs with over-coupled ones, the *ER*s of the GO-coated MRRs will increase compared to the uncoated MRRs, which can help improve the *NER* for the GO-coated device.

In **Figure 6d**, we plot the *NER* spectra at various P_{in} for the uncoated device. The corresponding results for the GO-coated device is shown in **Figure 6e**. The *NER* spectra were calculated by subtracting the backward transmission spectra from their corresponding forward transmission spectra. For the uncoated device, no obvious ONT behaviour was observed for P_{in} = ~-12.0 dBm, indicating the input CW power was not sufficient to induce any significant photo-thermal effects. By increasing the input CW power, the maximum *NER* value in the spectra increased to ~9.0 dB at P_{in} = ~-3.0 dBm, and then ~24.0 dB at P_{in} = ~6.0 dBm. Similar trends were also observed for the GO-coated device, where the ONT phenomenon was absent for P_{in} = ~-12.0 dBm and a maximum *NER* value of ~18.7 dB was achieved at P_{in} = ~-3.0 dBm.

Figure 6f shows the maximum *NER* versus P_{in} for both the uncoated and GO-coated devices. Compared to the uncoated device, the GO-coated device exhibited a lower power threshold for exhibiting the ONT behavior. At P_{in} = ~-9.0 dBm, the maximum *NER* values for the uncoated and GO-coated device were ~0.2 dB and ~3.0 dB, respectively. The curve for the GO-coated device increases more rapidly than that of the uncoated device. This reflects the fact that the GO-coated MRRs experienced a more significant wavelength shift resulting from photo-thermal effects.

7. Conclusion

In summary, we investigate the thermo-optic performance of silicon MRRs integrated with 2D GO films. We fabricate devices with precise control over the GO films' areas and thicknesses, and characterize the thermo-optic response induced by both environmental temperature changes and input coupled light power for devices with GO films of different thicknesses and degrees of reduction. Experimental results show that the GO-coated MRRs exhibit larger resonance wavelength shifts caused by environmental temperature variations compared to the uncoated MRRs. Conversely, the devices with reduced GO (rGO) exhibit the opposite behavior. In addition, we demonstrate an enhanced optical bistability as well as ONT induced by input coupled light in the hybrid MRRs. These results confirm the effectiveness of integrating 2D GO films onto silicon photonic platforms to implement high-performance thermo-optic devices and will have implications for a wide range of devices such as optical microcombs, [54 - 137] advanced circuits, [139-146] graphene oxide and other 2D material based devices, [147 - 173] and quantum optics. [174 - 189]

Notes

The authors declare no competing financial interest.

Data Availability Statement

The data that support the findings of this study are available from the corresponding author upon reasonable request.

References

[1] Q. Xu, B. Schmidt, S. Pradhan, and M. Lipson, "Micrometre-scale silicon electro-optic modulator," *Nature,* vol. 435, no. 7040, pp. 325-327, 2005/05/01, 2005.

[2] J. Riemensberger, N. Kuznetsov, J. Liu, J. He, R. N. Wang, and T. J. Kippenberg, "A photonic integrated continuous-travelling-wave parametric amplifier," *Nature,* vol. 612, no. 7938, pp. 56-61, 2022/12/01, 2022.

[3] Jiayang Wu, Tania Moein, Xingyuan Xu, Guanghui Ren, Arnan Mitchell, and David J. Moss, "Micro-ring resonator quality factor enhancement via an integrated Fabry-Perot cavity", Applied Physics Letters (APL) Photonics **2** 056103 (2017); doi: 10.1063/1.4981392.

[4] H. Shu, L. Chang, Y. Tao, B. Shen, W. Xie, M. Jin, A. Netherton, Z. Tao, X. Zhang, R. Chen, B. Bai, J. Qin, S. Yu, X. Wang, and J. E. Bowers, "Microcomb-driven silicon photonic systems," *Nature,* vol. 605, no. 7910, pp. 457-463, 2022/05/01, 2022.

[5] S. Sun, B. Wang, K. Liu, M. W. Harrington, F. Tabatabaei, R. Liu, J. Wang, S. Hanifi, J. S. Morgan, M. Jahanbozorgi, Z. Yang, S. M. Bowers, P. A. Morton, K. D. Nelson, A. Beling, D. J. Blumenthal, and X. Yi, "Integrated optical frequency division for microwave and mmWave generation," *Nature,* vol. 627, no. 8004, pp. 540-545, 2024/03/01, 2024.

[6] P. Marin-Palomo, J. N. Kemal, M. Karpov, A. Kordts, J. Pfeifle, M. H. P. Pfeiffer, P. Trocha, S. Wolf, V. Brasch, M. H. Anderson, R. Rosenberger, K. Vijayan, W. Freude, T. J. Kippenberg, and C. Koos, "Microresonator-based solitons for massively parallel coherent optical communications," *Nature,* vol. 546, no. 7657, pp. 274-279, 2017/06/01, 2017.

[7] Y. Li, W. Li, T. Han, X. Zheng, J. Li, B. Li, S. Fan, and C.-W. Qiu, "Transforming heat transfer with thermal metamaterials and devices," *Nature Reviews Materials,* vol. 6, no. 6, pp. 488-507, 2021/06/01, 2021.

[8] Yang Sun, Jiayang Wu, Mengxi Tan, Xingyuan Xu, Yang Li, Roberto Morandotti, Arnan Mitchell, and David J. Moss, "Applications of optical micro-combs", Advances in Optics and Photonics **15** (1) 86-175 (2023). https://doi.org/10.1364/AOP.470264.

[9] Q. Huang, H. Yu, Q. Zhang, Y. Li, W. Chen, Y. Wang, and J. Yang, "Thermally enhanced responsivity in an all-silicon optical power monitor based on defect-mediated absorption," *Photonics Research,* vol. 9, no. 11, pp. 2205-2213, 2021/11/01, 2021.

[10] M. Stegmaier, C. Rıos, H. Bhaskaran, and W. H. Pernice, "Thermo-optical effect in phase-change nanophotonics," *Acs Photonics,* vol. 3, no. 5, pp. 828-835, 2016.

[11] G. Ghosh, *Handbook of optical constants of solids: Handbook of thermo-optic coefficients of optical materials with applications*: Academic Press, 1998.

[12] D. Li, X. Liu, W. Li, Z. Lin, B. Zhu, Z. Li, J. Li, B. Li, S. Fan, J. Xie, and J. Zhu, "Scalable and hierarchically designed polymer film as a selective thermal emitter for high-performance all-day radiative cooling," *Nature Nanotechnology,* vol. 16, no. 2, pp. 153-158, 2021/02/01, 2021.

[13] L. Peng, D. Liu, H. Cheng, S. Zhou, and M. Zu, "A Multilayer Film Based Selective Thermal Emitter for Infrared Stealth Technology," *Advanced Optical Materials,* vol. 6, no. 23, pp. 1801006, 2018.

[14] D. M. Bierman, A. Lenert, W. R. Chan, B. Bhatia, I. Celanović, M. Soljačić, and E. N. Wang, "Enhanced photovoltaic energy conversion using thermally based spectral shaping," *Nature Energy,* vol. 1, no. 6, pp. 16068, 2016/05/23, 2016.

[15] M. L. Brongersma, Y. Cui, and S. Fan, "Light management for photovoltaics using high-index nanostructures," *Nature Materials,* vol. 13, no. 5, pp. 451-460, 2014/05/01, 2014.

[16] X. Xue, Y. Xuan, Y. Liu, P.-H. Wang, S. Chen, J. Wang, D. E. Leaird, M. Qi, and A. M. Weiner, "Mode-locked dark pulse Kerr combs in normal-dispersion microresonators," *Nature Photonics,* vol. 9, no. 9, pp. 594-600, 2015/09/01, 2015.

[17] M. Rowley, P.-H. Hanzard, A. Cutrona, H. Bao, S. T. Chu, B. E. Little, R. Morandotti, D. J. Moss, G.-L. Oppo, J. S. Totero Gongora, M. Peccianti, and A. Pasquazi, "Self-emergence of robust solitons in a microcavity," *Nature,* vol. 608, no. 7922, pp. 303-309, 2022/08/01, 2022.

[18] M. R. Watts, J. Sun, C. DeRose, D. C. Trotter, R. W. Young, and G. N. Nielson, "Adiabatic thermo-optic Mach-Zehnder switch," *Optics Letters,* vol. 38, no. 5, pp. 733-735, 2013/03/01, 2013.

[19] A. Densmore, S. Janz, R. Ma, J. H. Schmid, D.-X. Xu, A. Delâge, J. Lapointe, M. Vachon, and P. Cheben, "Compact and low power thermo-optic switch using folded silicon waveguides," *Optics Express,* vol. 17, no. 13, pp. 10457-10465, 2009/06/22, 2009.

[20] F. N. Hamada, M. Rosenzweig, K. Kang, S. R. Pulver, A. Ghezzi, T. J. Jegla, and P. A. Garrity, "An internal thermal sensor controlling temperature preference in Drosophila," *Nature,* vol. 454, no. 7201, pp. 217-220, 2008/07/01, 2008.

[21] Q. Hu, K.-T. Lin, H. Lin, Y. Zhang, and B. Jia, "Graphene Metapixels for Dynamically Switchable Structural Color," *ACS Nano,* vol. 15, no. 5, pp. 8930-8939, 2021/05/25, 2021.

[22] D. An, S. Cheng, Z. Zhang, C. Jiang, H. Fang, J. Li, Y. Liu, and C.-P. Wong, "A polymer-based thermal management material with enhanced thermal conductivity by introducing three-dimensional networks and covalent bond connections," *Carbon,* vol. 155, pp. 258-267, 2019/12/01/, 2019.

[23] W.-L. Song, P. Wang, L. Cao, A. Anderson, M. J. Meziani, A. J. Farr, and Y.-P. Sun, "Polymer/Boron Nitride Nanocomposite Materials for Superior Thermal Transport Performance," *Angewandte Chemie International Edition,* vol. 51, no. 26, pp. 6498-6501, 2012.

[24] H. Shen, J. Guo, H. Wang, N. Zhao, and J. Xu, "Bioinspired Modification of h-BN for High Thermal Conductive Composite Films with Aligned Structure," *ACS Applied Materials & Interfaces,* vol. 7, no. 10, pp. 5701-5708, 2015/03/18, 2015.

[25] D. L. Nika, and A. A. Balandin, "Two-dimensional phonon transport in graphene," *Journal of Physics: Condensed Matter,* vol. 24, no. 23, pp. 233203, 2012/05/04, 2012.

[26] A. A. Balandin, "Thermal properties of graphene and nanostructured carbon materials," *Nat. Mater.,* vol. 10, pp. 569, 2011.

[27] C. Zhi, Y. Bando, C. Tang, H. Kuwahara, and D. Golberg, "Large-Scale Fabrication of Boron Nitride Nanosheets and Their Utilization in Polymeric Composites with Improved Thermal and Mechanical Properties," *Advanced Materials,* vol. 21, no. 28, pp. 2889-2893, 2009.

[28] J. Wu, H. Lin, D. J. Moss, K. P. Loh, and B. Jia, "Graphene oxide for photonics, electronics and optoelectronics," *Nature Reviews Chemistry,* vol. 7, no. 3, pp. 162-183, 2023/03/01, 2023.

[29] J. Wu, L. Jia, Y. Zhang, Y. Qu, B. Jia, and D. J. Moss, "Graphene Oxide for Integrated Photonics and Flat Optics," *Advanced Materials,* vol. 33, no. 3, pp. 2006415, 2021.

[30] Y. Zhang, J. Wu, L. Jia, Y. Qu, Y. Yang, B. Jia, and D. J. Moss, "Graphene Oxide for Nonlinear Integrated Photonics," *Laser & Photonics Reviews,* vol. 17, no. 3, pp. 2200512, 2023/03/01, 2023.

[31] J. Hu, J. Wu, W. Liu, D. Jin, H. E. Dirani, S. Kerdiles, C. Sciancalepore, P. Demongodin, C. Grillet, C. Monat, D. Huang, B. Jia, and D. J. Moss, "2D graphene oxide: a versatile thermo-optic material," *Advanced Functional Materials,* vol. 34, no. 46, pp. 2406799, 2024.

[32] F. Bonaccorso, Z. Sun, T. Hasan, and A. C. Ferrari, "Graphene photonics and optoelectronics," *Nature Photonics,* vol. 4, no. 9, pp. 611-622, 2010/09/01, 2010.

[33] K. P. Loh, Q. Bao, G. Eda, and M. Chhowalla, "Graphene oxide as a chemically tunable platform for optical applications," *Nature Chemistry,* vol. 2, no. 12, pp. 1015-1024, 2010/12/01, 2010.

[34] Z. Luo, P. M. Vora, E. J. Mele, A. T. C. Johnson, and J. M. Kikkawa, "Photoluminescence and band gap modulation in graphene oxide," *Applied Physics Letters,* vol. 94, no. 11, 2009.

[35] Y.-L. Zhang, L. Guo, H. Xia, Q.-D. Chen, J. Feng, and H.-B. Sun, "Photoreduction of Graphene Oxides: Methods, Properties, and Applications," *Advanced Optical Materials,* vol. 2, no. 1, pp. 10-28, 2014.

[36] R. Jakhar, J. E. Yap, and R. Joshi, "Microwave reduction of graphene oxide," *Carbon,* vol. 170, pp. 277-293, 2020/12/01/, 2020.

[37] Y. Yang, Y. Zhang, J. Zhang, X. Zheng, Z. Gan, H. Lin, M. Hong, and B. Jia, "Graphene Metamaterial 3D Conformal Coating for Enhanced Light Harvesting," *ACS Nano,* vol. 17, no. 3, pp. 2611-2619, 2023/02/14, 2023.

[38] Y. Yang, H. Lin, B. Y. Zhang, Y. Zhang, X. Zheng, A. Yu, M. Hong, and B. Jia, "Graphene-based multilayered metamaterials with phototunable architecture for on-chip photonic devices," *Acs Photonics,* vol. 6, no. 4, pp. 1033-1040, 2019.

[39] H. Lin, Y. Song, Y. Huang, D. Kita, S. Deckoff-Jones, K. Wang, L. Li, J. Li, H. Zheng, Z. Luo, H. Wang, S. Novak, A. Yadav, C.-C. Huang, R.-J. Shiue, D. Englund, T. Gu, D. Hewak, K. Richardson, J. Kong, and J. Hu, "Chalcogenide glass-on-graphene photonics," *Nature Photonics,* vol. 11, no. 12, pp. 798-805, 2017/12/01, 2017.

[40] B. Radisavljevic, A. Radenovic, J. Brivio, V. Giacometti, and A. Kis, "Single-layer MoS2 transistors," *Nature Nanotechnology,* vol. 6, no. 3, pp. 147-150, 2011/03/01, 2011.

[41] Y. Zhang, J. Wu, Y. Yang, Y. Qu, L. Jia, T. Moein, B. Jia, and D. J. Moss, "Enhanced Kerr Nonlinearity and Nonlinear Figure of Merit in Silicon Nanowires Integrated with 2D Graphene Oxide Films," *ACS Applied Materials & Interfaces,* vol. 12, no. 29, pp. 33094-33103, 2020/07/22, 2020.

[42] Junkai Hu, Jiayang Wu, Di Jin, Wenbo Liu, Yuning Zhang, Yunyi Yang, Linnan Jia, Duan Huang, Baohua Jia, and David J. Moss, "Integrated waveguide and microring polarizers incorporating 2D reduced graphene oxide", ***Opto-Electronic Science*** **4** 240032 (2025). DOI: 10.29026/oes.2025.240032

[43] D. Jin, J. Wu, J. Hu, W. Liu, Y. Zhang, Y. Yang, L. Jia, D. Huang, B. Jia, and D. J. Moss, "Silicon photonic waveguide and microring resonator polarizers incorporating 2D graphene oxide films," *Applied Physics Letters,* vol. 125, no. 5, 2024.

[44] H. Arianfard, S. Juodkazis, D. J. Moss, and J. Wu, "Sagnac interference in integrated photonics," *Applied Physics Reviews,* vol. 10, no. 1, 2023.

[45] D. Jin, S. Ren, J. Hu, D. Huang, D. J. Moss, and J. Wu, "Modeling of Complex Integrated Photonic Resonators Using the Scattering Matrix Method," *Photonics,* vol. 11, no. 12, pp. 1107, 2024.

[46] H. Cai, Y. Cheng, H. Zhang, Q. Huang, J. Xia, R. Barille, and Y. Wang, "Enhanced linear absorption coefficient of in-plane monolayer graphene on a silicon microring resonator," *Optics Express,* vol. 24, no. 21, pp. 24105-24116, 2016/10/17, 2016.

[47] H. Li, Y. Anugrah, S. J. Koester, and M. Li, "Optical absorption in graphene integrated on silicon waveguides," *Applied Physics Letters,* vol. 101, no. 11, 2012.

[48] C. Horvath, D. Bachman, R. Indoe, and V. Van, "Photothermal nonlinearity and optical bistability in a graphene-silicon waveguide resonator," *Optics Letters,* vol. 38, no. 23, pp. 5036-5039, 2013/12/01, 2013.

[49] J. Wu, Y. Yang, Y. Qu, X. Xu, Y. Liang, S. T. Chu, B. E. Little, R. Morandotti, B. Jia, and D. J. Moss, "Graphene Oxide Waveguide and Micro-Ring Resonator Polarizers," *Laser & Photonics Reviews,* vol. 13, no. 9, pp. 1900056, 2019.

[50] J. Hu, J. Wu, D. Jin, S. T. Chu, B. E. Little, D. Huang, R. Morandotti, and D. J. Moss, "Thermo-Optic Response and Optical Bistablility of Integrated High-Index Doped Silica Ring Resonators," *Sensors,* vol. 23, no. 24, pp. 9767, 2023.

[51] P. W. Smith, and W. J. Tomlinson, "Bistable optical devices promise subpicosecond switching," *IEEE Spectrum,* vol. 18, pp. 26-33, June 01, 1981, 1981.

[52] H. Gibbs, "Optical Bistability: Controlling Light with Light, Academic Press," *Inc.: Orlando, FL, USA*, 1985.

[53] V. R. Almeida, and M. Lipson, "Optical bistability on a silicon chip," *Optics Letters,* vol. 29, no. 20, pp. 2387-2389, 2004/10/15, 2004.

[54] L. Fan, J. Wang, L. T. Varghese, H. Shen, B. Niu, Y. Xuan, A. M. Weiner, and M. Qi, "An All-Silicon Passive Optical Diode," *Science,* vol. 335, no. 6067, pp. 447-450, 2012/01/27, 2012.

[55] L. Bi, J. Hu, P. Jiang, D. H. Kim, G. F. Dionne, L. C. Kimerling, and C. A. Ross, "On-chip optical isolation in monolithically integrated non-reciprocal optical resonators," *Nature Photonics,* vol. 5, no. 12, pp. 758-762, 2011/12/01, 2011.

[56] M. Xu, J. Wu, T. Wang, X. Hu, X. Jiang, and Y. Su, "Push–Pull Optical Nonreciprocal Transmission in Cascaded Silicon Microring Resonators," *IEEE Photonics Journal,* vol. 5, no. 1, pp. 2200307-2200307, 2013.

[57] J. Wu, P. Cao, X. Hu, T. Wang, M. Xu, X. Jiang, F. Li, L. Zhou, and Y. Su, "Nested Configuration of Silicon Microring Resonator With Multiple Coupling Regimes," *IEEE Photonics Technology Letters,* vol. 25, no. 6, pp. 580-583, 2013.

58. Moss, D. J., Morandotti, R., Gaeta, A. L. & Lipson, M. New CMOS compatible platforms based on silicon nitride and Hydex for nonlinear optics. Nat. Photonics Vol. 7, 597-607 (2013).

59. L. Razzari, et al., "CMOS-compatible integrated optical hyper-parametric oscillator," Nature Photonics, vol. 4, no. 1, pp. 41-45, 2010.

60. A. Pasquazi, et al., "Sub-picosecond phase-sensitive optical pulse characterization on a chip", Nature Photonics, vol. 5, no. 10, pp. 618-623 (2011).

61. M Ferrera et al., "On-Chip ultra-fast 1st and 2nd order CMOS compatible all-optical integration", Optics Express vol. 19 (23), 23153-23161 (2011).

62. Bao, C., et al., Direct soliton generation in microresonators, Opt. Lett, 42, 2519 (2017).

63. M.Ferrera et al., “CMOS compatible integrated all-optical RF spectrum analyzer”, Optics Express, vol. 22, no. 18, 21488 - 21498 (2014).
64. M. Kues, et al., “Passively modelocked laser with an ultra-narrow spectral width”, Nature Photonics, vol. 11, no. 3, pp. 159, 2017.
65. M. Ferrera, et al., “Low-power continuous-wave nonlinear optics in doped silica glass integrated waveguide structures,” Nature Photonics, vol. 2, no. 12, pp. 737-740, 2008.
66. M.Ferrera et al.“On-Chip ultra-fast 1st and 2nd order CMOS compatible all-optical integration”, Opt. Express, vol. 19, (23)pp. 23153-23161 (2011).
67. D. Duchesne, M. Peccianti, M. R. E. Lamont, et al., “Supercontinuum generation in a high index doped silica glass spiral waveguide,” Optics Express, vol. 18, no, 2, pp. 923-930, 2010.
68. H Bao, L Olivieri, M Rowley, ST Chu, BE Little, R Morandotti, DJ Moss, ... “Turing patterns in a fiber laser with a nested microresonator: Robust and controllable microcomb generation”, Physical Review Research vol. 2 (2), 023395 (2020).
69. M. Ferrera, et al., “On-chip CMOS-compatible all-optical integrator”, Nature Communications, vol. 1, Article 29, 2010.
70. A. Pasquazi, et al., “All-optical wavelength conversion in an integrated ring resonator,” Optics Express, vol. 18, no. 4, pp. 3858-3863, 2010.
71. A.Pasquazi, Y. Park, J. Azana, et al., “Efficient wavelength conversion and net parametric gain via Four Wave Mixing in a high index doped silica waveguide,” Optics Express, vol. 18, no. 8, pp. 7634-7641, 2010.
72. Peccianti, M. Ferrera, L. Razzari, et al., “Subpicosecond optical pulse compression via an integrated nonlinear chirper,” Optics Express, vol. 18, no. 8, pp. 7625-7633, 2010.
73. M Ferrera, Y Park, L Razzari, BE Little, ST Chu, R Morandotti, DJ Moss, ... et al., “All-optical 1st and 2nd order integration on a chip”, Optics Express vol. 19 (23), 23153-23161 (2011).
74. M. Ferrera et al., “Low Power CW Parametric Mixing in a Low Dispersion High Index Doped Silica Glass Micro-Ring Resonator with Q-factor > 1 Million”, Optics Express, vol.17, no. 16, pp. 14098–14103 (2009).
75. M. Peccianti, et al., “Demonstration of an ultrafast nonlinear microcavity modelocked laser”, Nature Communications, vol. 3, pp. 765, 2012.
76. A.Pasquazi, et al., “Self-locked optical parametric oscillation in a CMOS compatible microring resonator: a route to robust optical frequency comb generation on a chip,” Optics Express, vol. 21, no. 11, pp. 13333-13341, 2013.
77. A.Pasquazi, et al., “Stable, dual mode, high repetition rate mode-locked laser based on a microring resonator,” Optics Express, vol. 20, no. 24, pp. 27355-27362, 2012.
78. Pasquazi, A. et al. Micro-combs: a novel generation of optical sources. Physics Reports 729, 1-81 (2018).
79. H. Bao, et al., Laser cavity-soliton microcombs, Nature Photonics, vol. 13, no. 6, pp. 384-389, Jun. 2019.

80. Antonio Cutrona, Maxwell Rowley, Debayan Das, Luana Olivieri, Luke Peters, Sai T. Chu, Brent L. Little, Roberto Morandotti, David J. Moss, Juan Sebastian Totero Gongora, Marco Peccianti, Alessia Pasquazi, "High Conversion Efficiency in Laser Cavity-Soliton Microcombs", Optics Express Vol. 30, Issue 22, pp. 39816-39825 (2022). https://doi.org/10.1364/OE.470376.

81. A. Cutrona, M. Rowley, A. Bendahmane, V. Cecconi,L. Peters, L. Olivieri, B. E. Little, S. T. Chu, S. Stivala, R. Morandotti, D. J. Moss, J. S. Totero-Gongora, M. Peccianti, A. Pasquazi, "Nonlocal bonding of a soliton and a blue-detuned state in a microcomb laser", ***Nature Communications Physics*** **6** Article 259 (2023). https://doi.org/10.1038/s42005-023-01372-0.

82. Aadhi A. Rahim, Imtiaz Alamgir, Luigi Di Lauro, Bennet Fischer, Nicolas Perron, Pavel Dmitriev, Celine Mazoukh, Piotr Roztocki, Cristina Rimoldi, Mario Chemnitz, Armaghan Eshaghi, Evgeny A. Viktorov, Anton V. Kovalev, Brent E. Little, Sai T. Chu, David J. Moss, and Roberto Morandotti, "Mode-locked laser with multiple timescales in a microresonator-based nested cavity", ***APL Photonics*** **9** 031302 (2024). DOI:10.1063/5.0174697.

83. Andrew Cooper, Luana Olivieri, Antonio Cutrona, Debayan Das, Luke Peters, Sai Tak Chu, Brent Little, Roberto Morandotti, David J Moss, Marco Peccianti, and Alessia Pasquazi, "Parametric interaction of laser cavity-solitons with an external CW pump", ***Optics Express*** **32** (12), 21783-21794 (2024).

84. A. Cutrona, M. Rowley, A. Bendahmane, V. Cecconi,L. Peters, L. Olivieri, B. E. Little, S. T. Chu, S. Stivala, R. Morandotti, D. J. Moss, J. S. Totero-Gongora, M. Peccianti, A. Pasquazi, "Stability Properties of Laser Cavity-Solitons for Metrological Applications", Applied Physics Letters vol. 122 (12) 121104 (2023); doi: 10.1063/5.0134147.

85. Caitlin E. Murray, Mengxi Tan, Chawaphon Prayoonyong, Sai T. Chu, Brent E. Little, Roberto Morandotti, Arnan Mitchell, David J. Moss and Bill Corcoran, "Investigating the thermal robustness of soliton crystal microcombs", ***Optics Express*** **31**(23), 37749-37762 (2023).

86. Yonghang Sun, James Salamy, Caitlin E. Murry, Brent E. Little, Sai T. Chu, Roberto Morandotti, Arnan Mitchell, David J. Moss, Bill Corcoran, "Enhancing laser temperature stability by passive self-injection locking to a micro-ring resonator", ***Optics Express*** **32** (13) 23841-23855 (2024) https://doi.org/10.1364/OE.515269.

87. Yonghang Sun, James Salamy, Caitlin E. Murray, Xiaotian Zhu, Brent E. Little, Roberto Morandotti, Arnan Mitchell, Sai T. Chu, David J. Moss, Bill Corcoran, "Self-locking of free-running DFB lasers to a single microring resonator for dense WDM", ***Journal of Lightwave Technology*** **43**, (4) 1995-2002 (2025). DOI: 10.1109/JLT.2024.3494694.

88. X. Xu, J. Wu, M. Shoeiby, T. G. Nguyen, S. T. Chu, B. E. Little, R. Morandotti, A. Mitchell, and D. J. Moss, "Reconfigurable broadband microwave photonic intensity differentiator based on an integrated optical frequency comb source," APL Photonics, vol. 2, no. 9, 096104, Sep. 2017.

89. Xu, X., et al., Photonic microwave true time delays for phased array antennas using a 49 GHz FSR integrated micro-comb source, Photonics Research, vol. 6, B30-B36 (2018).

90. X. Xu, M. Tan, J. Wu, R. Morandotti, A. Mitchell, and D. J. Moss, “Microcomb-based photonic RF signal processing”, IEEE Photonics Technology Letters, vol. 31 no. 23 1854-1857, 2019.
91. Xu, et al., “Advanced adaptive photonic RF filters with 80 taps based on an integrated optical micro-comb source,” Journal of Lightwave Technology, vol. 37, no. 4, pp. 1288-1295 (2019).
92. X. Xu, et al., “Photonic RF and microwave integrator with soliton crystal microcombs”, IEEE Transactions on Circuits and Systems II: Express Briefs, vol. 67, no. 12, pp. 3582-3586, 2020. DOI:10.1109/TCSII.2020.2995682.
93. X. Xu, et al., “High performance RF filters via bandwidth scaling with Kerr micro-combs,” APL Photonics, vol. 4 (2) 026102. 2019.
94. M. Tan, et al., “Microwave and RF photonic fractional Hilbert transformer based on a 50 GHz Kerr micro-comb”, Journal of Lightwave Technology, vol. 37, no. 24, pp. 6097 – 6104, 2019.
95. M. Tan, et al., “RF and microwave fractional differentiator based on photonics”, IEEE Transactions on Circuits and Systems: Express Briefs, vol. 67, no.11, pp. 2767-2771, 2020. DOI:10.1109/TCSII.2020.2965158.
96. M. Tan, et al., “Photonic RF arbitrary waveform generator based on a soliton crystal micro-comb source”, Journal of Lightwave Technology, vol. 38, no. 22, pp. 6221-6226 (2020). DOI: 10.1109/JLT.2020.3009655.
97. M. Tan, X. Xu, J. Wu, R. Morandotti, A. Mitchell, and D. J. Moss, “RF and microwave high bandwidth signal processing based on Kerr Micro-combs”, Advances in Physics X, VOL. 6, NO. 1, 1838946 (2021). DOI:10.1080/23746149.2020.1838946.
98. X. Xu, et al., “Advanced RF and microwave functions based on an integrated optical frequency comb source,” Opt. Express, vol. 26 (3) 2569 (2018).
99. M. Tan, X. Xu, J. Wu, B. Corcoran, A. Boes, T. G. Nguyen, S. T. Chu, B. E. Little, R. Morandotti, A. Lowery, A. Mitchell, and D. J. Moss, “"Highly Versatile Broadband RF Photonic Fractional Hilbert Transformer Based on a Kerr Soliton Crystal Microcomb”, Journal of Lightwave Technology vol. 39 (24) 7581-7587 (2021).
100. Wu, J. et al. RF Photonics: An Optical Microcombs’ Perspective. IEEE Journal of Selected Topics in Quantum Electronics Vol. 24, 6101020, 1-20 (2018).
101. T. G. Nguyen et al., “Integrated frequency comb source-based Hilbert transformer for wideband microwave photonic phase analysis,” Opt. Express, vol. 23, no. 17, pp. 22087-22097, Aug. 2015.
102. X. Xu, et al., “Broadband RF channelizer based on an integrated optical frequency Kerr comb source,” Journal of Lightwave Technology, vol. 36, no. 19, pp. 4519-4526, 2018.
103. X. Xu, et al., “Continuously tunable orthogonally polarized RF optical single sideband generator based on micro-ring resonators,” Journal of Optics, vol. 20, no. 11, 115701. 2018.

104. X. Xu, et al., “Orthogonally polarized RF optical single sideband generation and dual-channel equalization based on an integrated microring resonator,” Journal of Lightwave Technology, vol. 36, no. 20, pp. 4808-4818. 2018.
105. X. Xu, et al., “Photonic RF phase-encoded signal generation with a microcomb source”, J. Lightwave Technology, vol. 38, no. 7, 1722-1727, 2020.
106. X. Xu, et al., Broadband microwave frequency conversion based on an integrated optical micro-comb source”, Journal of Lightwave Technology, vol. 38 no. 2, pp. 332-338, 2020.
107. M. Tan, et al., “Photonic RF and microwave filters based on 49GHz and 200GHz Kerr microcombs”, Optics Comm. vol. 465,125563, Feb. 22. 2020.
108. X. Xu, et al., “Broadband photonic RF channelizer with 90 channels based on a soliton crystal microcomb”, Journal of Lightwave Technology, Vol. 38, no. 18, pp. 5116 – 5121 (2020). doi: 10.1109/JLT.2020.2997699.
109. M. Tan et al, “Orthogonally polarized Photonic Radio Frequency single sideband generation with integrated micro-ring resonators”, IOP Journal of Semiconductors, Vol. 42 (4), 041305 (2021). DOI: 10.1088/1674-4926/42/4/041305.
110. Mengxi Tan, X. Xu, J. Wu, T. G. Nguyen, S. T. Chu, B. E. Little, R. Morandotti, A. Mitchell, and David J. Moss, “Photonic Radio Frequency Channelizers based on Kerr Optical Micro-combs”, IOP Journal of Semiconductors Vol. 42 (4), 041302 (2021). DOI:10.1088/1674-4926/42/4/041302.
111. B. Corcoran, et al., “Ultra-dense optical data transmission over standard fiber with a single chip source”, Nature Communications, vol. 11, Article:2568, 2020.
112. X. Xu et al, “Photonic perceptron based on a Kerr microcomb for scalable high speed optical neural networks”, Laser and Photonics Reviews, vol. 14, no. 8, 2000070 (2020). DOI: 10.1002/lpor.202000070.
113. X. Xu, et al., “11 TOPs photonic convolutional accelerator for optical neural networks”, Nature vol. 589, 44-51 (2021).
114. Xingyuan Xu, Weiwei Han, Mengxi Tan, Yang Sun, Yang Li, Jiayang Wu, Roberto Morandotti, Arnan Mitchell, Kun Xu, and David J. Moss, “Neuromorphic computing based on wavelength-division multiplexing”, ***IEEE Journal of Selected Topics in Quantum Electronics*** **29** (2) 7400112 (2023). DOI:10.1109/JSTQE.2022.3203159.
115. Yunping Bai, Xingyuan Xu,1, Mengxi Tan, Yang Sun, Yang Li, Jiayang Wu, Roberto Morandotti, Arnan Mitchell, Kun Xu, and David J. Moss, “Photonic multiplexing techniques for neuromorphic computing”, Nanophotonics vol. 12 (5): 795–817 (2023). DOI:10.1515/nanoph-2022-0485.
116. Chawaphon Prayoonyong, Andreas Boes, Xingyuan Xu, Mengxi Tan, Sai T. Chu, Brent E. Little, Roberto Morandotti, Arnan Mitchell, David J. Moss, and Bill Corcoran, “Frequency comb distillation for optical superchannel transmission”, Journal of Lightwave Technology vol. 39 (23) 7383-7392 (2021). DOI: 10.1109/JLT.2021.3116614.
117. Mengxi Tan, Xingyuan Xu, Jiayang Wu, Bill Corcoran, Andreas Boes, Thach G. Nguyen, Sai T. Chu, Brent E. Little, Roberto Morandotti, Arnan Mitchell, and David J. Moss, “Integral order photonic RF signal processors based on a soliton crystal micro-comb

source", IOP Journal of Optics vol. 23 (11) 125701 (2021). https://doi.org/10.1088/2040-8986/ac2eab

118. Yang Sun, Jiayang Wu, Yang Li, Xingyuan Xu, Guanghui Ren, Mengxi Tan, Sai Tak Chu, Brent E. Little, Roberto Morandotti, Arnan Mitchell, and David J. Moss, "Optimizing the performance of microcomb based microwave photonic transversal signal processors", Journal of Lightwave Technology vol. 41 (23) pp 7223-7237 (2023). DOI: 10.1109/JLT.2023.3314526.
119. Mengxi Tan, Xingyuan Xu, Andreas Boes, Bill Corcoran, Thach G. Nguyen, Sai T. Chu, Brent E. Little, Roberto Morandotti, Jiayang Wu, Arnan Mitchell, and David J. Moss, "Photonic signal processor for real-time video image processing based on a Kerr microcomb", ***Nature Communications Engineering*** **2** 94 (2023). DOI:10.1038/s44172-023-00135-7.
120. Mengxi Tan, Xingyuan Xu, Jiayang Wu, Roberto Morandotti, Arnan Mitchell, and David J. Moss, "Photonic RF and microwave filters based on 49GHz and 200GHz Kerr microcombs", Optics Communications, vol. 465, Article: 125563 (2020). doi:10.1016/j.optcom.2020.125563. doi.org/10.1063/1.5136270.
121. Yang Sun, Jiayang Wu, Yang Li, Mengxi Tan, Xingyuan Xu, Sai Chu, Brent Little, Roberto Morandotti, Arnan Mitchell, and David J. Moss, "Quantifying the Accuracy of Microcomb-based Photonic RF Transversal Signal Processors", IEEE Journal of Selected Topics in Quantum Electronics vol. 29 no. 6, pp. 1-17, Art no. 7500317 (2023). 10.1109/JSTQE.2023.3266276.
122. Yang Li, Yang Sun, Jiayang Wu, Guanghui Ren, Bill Corcoran, Xingyuan Xu, Sai T. Chu, Brent. E. Little, Roberto Morandotti, Arnan Mitchell, and David J. Moss, "Processing accuracy of microcomb-based microwave photonic signal processors for different input signal waveforms", ***MDPI Photonics*** ***10***, 10111283 (2023). DOI:10.3390/photonics10111283
123. Yang Sun, Jiayang Wu, Yang Li, and David J. Moss, "Comparison of microcomb-based RF photonic transversal signal processors implemented with discrete components versus integrated chips", ***MDPI Micromachines*** **14**, 1794 (2023). https://doi.org/10.3390/mi14091794
124. Mengxi Tan, David J. Moss, "The laser trick that could put an ultraprecise optical clock on a chip", ***Nature*** **624**, (7991) 256-257 (2023). *doi.org/10.1038/d41586-023-03782-0.*
125. Weiwei Han, Zhihui Liu, Yifu Xu, Mengxi Tan, Chaoran Huang, Jiayang Wu, Kun Xu, David J. Moss, and Xingyuan Xu, "Photonic RF Channelization Based on Microcombs", ***IEEE Journal of Selected Topics in Quantum Electronics*** **30** (5) 7600417 (2024). DOI:10.1109/JSTQE.2024.3398419.
126. Yang Li, Yang Sun, Jiayang Wu, Guanghui Ren, Xingyuan Xu, Mengxi Tan, Sai Chu, Brent Little, Roberto Morandotti, Arnan Mitchell, and David Moss, "Feedback control in micro-comb-based microwave photonic transversal filter systems", ***IEEE Journal of Selected Topics in Quantum Electronics*** Vol. **30** (5) 2900117 (2024). DOI: 10.1109/JSTQE.2024.3377249.

127. Weiwei Han, Zhihui Liu, Yifu Xu, Mengxi Tan, Yuhua Li, Xiaotian Zhu, Yanni Ou, Feifei Yin, Roberto Morandotti, Brent E. Little, Sai Tak Chu, Xingyuan Xu, David J. Moss, and Kun Xu, "Dual-polarization RF Channelizer Based on Microcombs", ***Optics Express*** **32**, No. 7, 11281-11295 (2024). DOI: 10.1364/OE.519235.

128. Zhihui Liu, Haoran Zhang, Yuhang Song, Xiaotian Zhu, Yunping Bai, Mengxi Tan, Bill Corcoran, Caitlin Murphy, Sai T. Chu, David J. Moss, Xingyuan Xu, and Kun Xu, "Advances in Soliton Crystals Microcombs", Photonics Vol. 11, 1164 (2024). https://doi.org/10.3390/photonics11121164.

129. C. Mazoukh, L. Di Lauro, I. Alamgir1 B. Fischer, A. Aadhi, A. Eshaghi, B. E. Little, S. T. Chu, D. J. Moss, and R. Morandotti, "Genetic algorithm-enhanced microcomb state generation", ***Nature Communications Physics*** Vol. 7, Article: 81 (2024). DOI: 10.1038/s42005-024-01558-0.

130. Shifan Chen, Yixuan Zheng, Yifu Xu, Xiaotian Zhu, Sirui Huang, Shuai Wang, Xiaoyan Xu, Chengzhuo Xia, Zhihui Liu, Chaoran Huang, Roberto Morandotti, Sai T. Chu, Brent E. Little, Bill Corcoran, Yuyang Liu, Yunping Bai, David J. Moss, Xingyuan Xu, and Kun Xu, "High-bit-efficiency TOPS optical tensor convolutional accelerator using micro-combs", ***Laser & Photonics Reviews*** **19** 2401975 (2025). DOI: 10.1002/lpor.202401975

131. Weiwei Han, Zhihui Liu, Yifu Xu, Mengxi Tan, Yuhua Li, Xiaotian Zhu, Yanni Ou, Feifei Yin, Roberto Morandotti, Brent E. Little, Sai Tak Chu, David J. Moss, Xingyuan Xu, and Kun Xu, "TOPS-speed complex-valued convolutional accelerator for feature extraction and inference", ***Nature Communications*** **16** 292 (2025). DOI: 10.1038/s41467-024-55321-8.

132. Yang Li, Yang Sun, Jiayang Wu, Guanghui Ren, Roberto Morandotti, Xingyuan Xu, Mengxi Tan, Arnan Mitchell, and David J. Moss, "Performance analysis of microwave photonic spectral filters based on optical microcombs", ***Advanced Physics Research*** **4** (9) 2400084 (2025). DOI:10.1002/apxr.202400084.

133. Luigi di Lauro, Stefania Sciara, Bennet Fischer, Junliang Dong, Imtiaz Alamgir, Benjamin Wetzel, Goëry Genty, Mitchell Nichols, Armaghan Eshaghi, David J. Moss, Roberto Morandotti, "Optimization Methods for Integrated and Programmable Photonics in Next-Generation Classical and Quantum Smart Communication and Signal Processing", ***Advances in Optics and Photonics*** Vol. **17** (2) (2025).

134. Bill Corcoran, Arnan Mitchell, Roberto Morandotti, Leif K. Oxenlowe, and David J. Moss, "Optical microcombs for ultrahigh-bandwidth communications", ***Nature Photonics*** Volume **19** Issue 5 May (2025). DOI: 10.1038/s41566-025-01662-9.

135. Qihang Ai, Mengxi Tan, Hanxiao Feng, Xinyu Yang, Xingyuan Xu, Roberto Morandotti, Arnan Mitchell, Donglin Su, and David J. Moss, "Photonic real-time signal processing", ***Nanophotonics*** **29** (2025).

136. Xingyuan Xu, Jiajia Wang, Xiaotian Zhu, Yifu Xu, Shifan Chen, Haoran Zhang, Shuying Li, Yunping Bai, Zhihui Liu, Roberto Morandotti, Brent E. Little, Arthur J. Lowery, David J. Moss, Sai T. Chu, and Kun Xu, "Microcomb-enabled parallel self- calibration optical convolution streaming processor", ***Light Science and Applications*** (2025).

137. Shifan Chen, Yixuan Zheng, Yifu Xu, Xiaotian Zhu, Sirui Huang, Shuai Wang, Xiaoyan Xu, Chengzhuo Xia, Zhihui Liu, Chaoran Huang, Roberto Morandotti, Sai T. Chu, Brent E. Little, Bill Corcoran, Yuyang Liu, Yunping Bai, David J. Moss, Xingyuan Xu, and Kun Xu, "Integrated photonic neural networks", ***npj Nanophotonics*** **2**, 28 (2025).

138. A. Aadhi, L. Di Lauro, B. Fischer, P. Dmitriev, I. Alamgir, C. Mazoukh, N. Perron, E. Viktorov, A. Kovalev, A. Eshaghi, S. Vakili, M. Chemnitz, P. Roztocki, B.E. Little, S. T. Chu, D. J. Moss, and R. Morandotti, "Scalable Photonic Reservoir for Parallel Machine Learning Applications", ***Nature Communications*** **16** (2025).

139. Hamed Arianfard, Saulius Juodkazis, David J. Moss, and Jiayang Wu, "Sagnac interference in integrated photonics", ***Applied Physics Reviews*** **10** (1) 011309 (2023). doi: 10.1063/5.0123236.

140. Hamed Arianfard, Jiayang Wu, Saulius Juodkazis, and David J. Moss, "Optical analogs of Rabi splitting in integrated waveguide-coupled resonators", ***Advanced Physics Research*** **2** 2200123 (2023). DOI: 10.1002/apxr.202200123.

141. Hamed Arianfard, Jiayang Wu, Saulius Juodkazis, and David J. Moss, "Spectral shaping based on optical waveguides with advanced Sagnac loop reflectors", Paper No. PW22O-OE201-20, SPIE-Opto, Integrated Optics: Devices, Materials, and Technologies XXVI, SPIE Photonics West, San Francisco CA January 22 - 27 (2022). doi: 10.1117/12.2607902

142. Hamed Arianfard, Jiayang Wu, Saulius Juodkazis, David J. Moss, "Spectral Shaping Based on Integrated Coupled Sagnac Loop Reflectors Formed by a Self-Coupled Wire Waveguide", IEEE Photonics Technology Letters vol. 33 (13) 680-683 (2021). DOI:10.1109/LPT.2021.3088089.

143. Hamed Arianfard, Jiayang Wu, Saulius Juodkazis and David J. Moss, "Three Waveguide Coupled Sagnac Loop Reflectors for Advanced Spectral Engineering", Journal of Lightwave Technology vol. 39 (11) 3478-3487 (2021). DOI: 10.1109/JLT.2021.3066256.

144. Hamed Arianfard, Jiayang Wu, Saulius Juodkazis and David J. Moss, "Advanced Multi-Functional Integrated Photonic Filters based on Coupled Sagnac Loop Reflectors", Journal of Lightwave Technology vol. 39 Issue: 5, pp.1400-1408 (2021). DOI:10.1109/JLT.2020.3037559.

145. Hamed Arianfard, Jiayang Wu, Saulius Juodkazis and David J. Moss, "Advanced multi-functional integrated photonic filters based on coupled Sagnac loop reflectors", Paper 11691-4, PW21O-OE203-44, Silicon Photonics XVI, SPIE Photonics West, San Francisco CA March 6-11 (2021). doi.org/10.1117/12.2584020

146. Jiayang Wu, Tania Moein, Xingyuan Xu, and David J. Moss, "Advanced photonic filters via cascaded Sagnac loop reflector resonators in silicon-on-insulator integrated nanowires", Applied Physics Letters Photonics vol. 3 046102 (2018). DOI:/10.1063/1.5025833

147. Yunyi Yang, Jiayang Wu, Xingyuan Xu, Sai T. Chu, Brent E. Little, Roberto Morandotti, Baohua Jia, and David J. Moss, "Enhanced four-wave mixing in graphene oxide coated

waveguides", Applied Physics Letters Photonics vol. 3 120803 (2018). doi: 10.1063/1.5045509.

148. Wu, J. et al., "Graphene oxide waveguide and micro-ring resonator polarizers", Laser and Photonics Reviews Vol. 13, 1900056 (2019).

149. Jiayang Wu, Yunyi Yang, Yang Qu, Xingyuan Xu, Yao Liang, Sai T. Chu, Brent E. Little, Roberto Morandotti, Baohua Jia, and David J. Moss, "Graphene oxide waveguide polarizers and polarization selective micro-ring resonators", Laser and Photonics Reviews vol. 13 (9) 1900056 (2019). DOI:10.1002/lpor.201900056.

150. Wu, J. et al. "2D layered graphene oxide films integrated with micro-ring resonators for enhanced nonlinear optics", Small Vol. 16, 1906563 (2020).

151. Yang Qu, Jiayang Wu, Yunyi Yang, Yuning Zhang, Yao Liang, Houssein El Dirani, Romain Crochemore, Pierre Demongodin, Corrado Sciancalepore, Christian Grillet, Christelle Monat, Baohua Jia, and David J. Moss, "Enhanced nonlinear four-wave mixing in silicon nitride waveguides integrated with 2D layered graphene oxide films", Advanced Optical Materials vol. 8 (21) 2001048 (2020). DOI: 10.1002/adom.202001048. arXiv:2006.14944.

152. Jiayang Wu, Yunyi Yang, Yang Qu, Yuning Zhang, Linnan Jia, Xingyuan Xu, Sai T. Chu, Brent E. Little, Roberto Morandotti, Baohua Jia, and David J. Moss, "Enhanced nonlinear four-wave mixing in microring resonators integrated with layered graphene oxide films", Small vol. 16 (16) 1906563 (2020). DOI: 10.1002/smll.201906563

153. Jiayang Wu, Yunyi Yang, Yang Qu, Xingyuan Xu, Yao Liang, Sai T. Chu, Brent E. Little, Roberto Morandotti, Baohua Jia, and David J. Moss, "Graphene oxide waveguide polarizers and polarization selective micro-ring resonators", Paper 11282-29, SPIE Photonics West, San Francisco, CA, 4 - 7 February (2020). doi: 10.1117/12.2544584

154. Yuning Zhang, Jiayang Wu, Yang Qu, Linnan Jia, Baohua Jia, and David J. Moss, "Design and optimization of four-wave mixing in microring resonators integrated with 2D graphene oxide films", Journal of Lightwave Technology Vol. 39 (20) 6553-6562 (2021). DOI:10.1109/JLT.2021.3101292.

155. Yang Qu, Jiayang Wu, Yuning Zhang, Yao Liang, Baohua Jia, and David J. Moss, "Analysis of four-wave mixing in silicon nitride waveguides integrated with 2D layered graphene oxide films", Journal of Lightwave Technology Vol. 39 (9) 2902-2910 (2021). DOI: 10.1109/JLT.2021.3059721.

156. Y. Qu, J. Wu, Y. Zhang, L. Jia, Y. Yang, X. Xu, S. T. Chu, B. E. Little, R. Morandotti, B. Jia, and D. J. Moss, "Graphene oxide for enhanced optical nonlinear performance in CMOS compatible integrated devices", Paper No. 11688-30, PW21O-OE109-36, 2D Photonic Materials and Devices IV, SPIE Photonics West, San Francisco CA March 6-11 (2021). doi.org/10.1117/12.2583978

157. Yuning Zhang, Jiayang Wu, Yang Qu, Linnan Jia, Baohua Jia, and David J. Moss, "Optimizing the Kerr nonlinear optical performance of silicon waveguides integrated with 2D graphene oxide films", Journal of Lightwave Technology Vol. 39 (14) 4671-4683 (2021). DOI: 10.1109/JLT.2021.3069733.

158. Yang Qu, Jiayang Wu, Yuning Zhang, Yunyi Yang, Linnan Jia, Baohua Jia, and David J. Moss, "Photo thermal tuning in GO-coated integrated waveguides", Micromachines Vol. 13 1194 (2022). doi.org/10.3390/mi13081194

159. Zhang Y, Wu J, Qu Y, Jia L, Jia B, D.J. Moss, "Graphene oxide-based waveguides for enhanced self-phase modulation", Annals of Mathematics and Physics Vol. 5 (2) 103-106 (2022). DOI:10.17352/amp.000048

160. Yuning Zhang, Jiayang Wu, Yunyi Yang, Yang Qu, Linnan Jia, Baohua Jia, and David J. Moss, "Enhanced spectral broadening of femtosecond optical pulses in silicon nanowires integrated with 2D graphene oxide films", Micromachines Vol. 13 756 (2022). DOI:10.3390/mi13050756.

161. Yuning Zhang, Jiayang Wu, Yunyi Yang, Yang Qu, Linnan Jia, Houssein El Dirani, Sébastien Kerdiles, Corrado Sciancalepore, Pierre Demongodin, Christian Grillet, Christelle Monat, Baohua Jia, and David J. Moss, "Enhanced supercontinuum generated in SiN waveguides coated with GO films", ***Advanced Materials Technologies*** **8** (1) 2201796 (2023). DOI:10.1002/admt.202201796.

162. Yuning Zhang, Jiayang Wu, Yunyi Yang, Yang Qu, Houssein El Dirani, Romain Crochemore, Corrado Sciancalepore, Pierre Demongodin, Christian Grillet, Christelle Monat, Baohua Jia, and David J. Moss, "Enhanced self-phase modulation in silicon nitride waveguides integrated with 2D graphene oxide films", IEEE Journal of Selected Topics in Quantum Electronics Vol. 29 (1) 5100413 (2023). DOI: 10.1109/JSTQE.2022.3177385

163. Yang Qu, Jiayang Wu, Yuning Zhang, Yunyi Yang, Linnan Jia, Houssein El Dirani, Sébastien Kerdiles, Corrado Sciancalepore, Pierre Demongodin, Christian Grillet, Christelle Monat, Baohua Jia, and David J. Moss, "Integrated optical parametric amplifiers in silicon nitride waveguides incorporated with 2D graphene oxide films", ***Light: Advanced Manufacturing*** **4** 39 (2023). https://doi.org/10.37188/lam.2023.039.

164. Jiayang Wu, Yuning Zhang, Junkai Hu, Yunyi Yang, Di Jin, Wenbo Liu, Duan Huang, Baohua Jia, David J. Moss, "Novel functionality with 2D graphene oxide films integrated on silicon photonic chips", ***Advanced Materials*** Vol. 36 2403659 (2024). DOI: 10.1002/adma.202403659.

165. Di Jin, Jiayang Wu, Junkai Hu, Wenbo Liu, Yuning Zhang, Yunyi Yang, Linnan Jia, Duan Huang, Baohua Jia, and David J. Moss, "Silicon photonic waveguide and microring resonator polarizers incorporating 2D graphene oxide films", Applied Physics Letters, Vol. 125, 053101 (2024). doi: 10.1063/5.0221793.

166. Yuning Zhang, Jiayang Wu, Linnan Jia, Di Jin, Baohua Jia, Xiaoyong Hu, David Moss, Qihuang Gong, "Advanced optical polarizers based on 2D materials", ***npj Nanophotonics*** **1**, 28 (2024). DOI: 10.1038/s44310-024-00028-3.

167. Y. Zhang, J. Wu, Y. Yang,Y. Qu, L. Jia, C. Grillet, C. Monat, B. Jia, and D.J. Moss, "Graphene oxide for enhanced nonlinear optics in integrated photonic chips", Paper 12888-16, Conference OE109, 2D Photonic Materials and Devices VII, Chair(s): Arka Majmdar; Carlos M. Torres Jr.; Hui Deng, SPIE Photonics West, San Francisco CA,

January 27 – February 1 (2024). Proceedings Volume 12888, 2D Photonic Materials and Devices VII; 1288805 (2024). https://doi.org/10.1117/12.3005069

168. Di Jin, Wenbo Liu, Linnan Jia, Junkai Hu, Duan Huang, Jiayang Wu, Baohua Jia, and David J. Moss, "Thickness and Wavelength Dependent Nonlinear Optical Absorption in 2D Layered MXene Films", ***Small Science*** **4** 2400179 (2024). DOI:10.1002/smsc202400179;
169. Yuning Zhang, Jiayang Wu, Junkai Hu, Linnan Jia, Di Jin, Baohua Jia, Xiaoyong Hu, David J. Moss, Qihuang Gong, "2D material integrated photonics: towards industrial manufacturing and commercialization", Applied Physics Letters Photonics **10**, 000000 (2025); doi: 10.1063/5.0249703.
170. Linnan Jia, Yang Qu, Jiayang Wu, Yuning Zhang, Yunyi Yang, Baohua Jia, and David J. Moss, "Third-order optical nonlinearities of 2D materials at telecommunications wavelengths", ***Micromachines***, **14** 307 (2023). https://doi.org/10.3390/mi14020307.
171. Linnan Jia, Jiayang Wu, Yuning Zhang, Yang Qu, Baohua Jia, Zhigang Chen, and David J. Moss, "Fabrication Technologies for the On-Chip Integration of 2D Materials", Small: Methods Vol. 6, 2101435 (2022). DOI:10.1002/smtd.202101435.
172. Linnan Jia, Dandan Cui, Jiayang Wu, Haifeng Feng, Tieshan Yang, Yunyi Yang, Yi Du, Weichang Hao, Baohua Jia, David J. Moss, "BiOBr nanoflakes with strong nonlinear optical properties towards hybrid integrated photonic devices", Applied Physics Letters Photonics vol. 4 090802 vol. (2019). DOI: 10.1063/1.5116621
173. Linnan Jia, Jiayang Wu, Yunyi Yang, Yi Du, Baohua Jia, David J. Moss, "Large Third-Order Optical Kerr Nonlinearity in Nanometer-Thick PdSe2 2D Dichalcogenide Films: Implications for Nonlinear Photonic Devices", ACS Applied Nano Materials vol. 3 (7) 6876–6883 (2020). DOI:10.1021/acsanm.0c01239.
174. Kues, M. et al. "Quantum optical microcombs", Nature Photonics vol. 13, (3) 170-179 (2019). doi:10.1038/s41566-019-0363-0
175. C.Reimer, L. Caspani, M. Clerici, et al., "Integrated frequency comb source of heralded single photons," Optics Express, vol. 22, no. 6, pp. 6535-6546, 2014.
176. C. Reimer, et al., "Cross-polarized photon-pair generation and bi-chromatically pumped optical parametric oscillation on a chip", Nature Communications, vol. 6, Article 8236, 2015. DOI: 10.1038/ncomms9236.
177. L. Caspani, C. Reimer, M. Kues, et al., "Multifrequency sources of quantum correlated photon pairs on-chip: a path toward integrated Quantum Frequency Combs," Nanophotonics, vol. 5, no. 2, pp. 351-362, 2016.
178. C. Reimer et al., "Generation of multiphoton entangled quantum states by means of integrated frequency combs," Science, vol. 351, no. 6278, pp. 1176-1180, 2016.
179. M. Kues, et al., "On-chip generation of high-dimensional entangled quantum states and their coherent control", Nature, vol. 546, no. 7660, pp. 622-626, 2017.
180. P. Roztocki et al., "Practical system for the generation of pulsed quantum frequency combs," Optics Express, vol. 25, no. 16, pp. 18940-18949, 2017.

181. Y. Zhang, et al., “Induced photon correlations through superposition of two four-wave mixing processes in integrated cavities”, Laser and Photonics Reviews, vol. 14, no. 7, pp. 2000128, 2020. DOI: 10.1002/lpor.202000128
182. C. Reimer, et al., “High-dimensional one-way quantum processing implemented on d-level cluster states”, Nature Physics, vol. 15, no.2, pp. 148–153, 2019.
183. P.Roztocki et al., “Complex quantum state generation and coherent control based on integrated frequency combs”, Journal of Lightwave Technology vol. 37 (2) 338-347 (2019).
184. S. Sciara et al., “Generation and Processing of Complex Photon States with Quantum Frequency Combs”, IEEE Photonics Technology Letters vol. 31 (23) 1862-1865 (2019). DOI: 10.1109/LPT.2019.2944564.
185. Nicola Montaut, Agnes George, Monika Monika, Farzam Nosrati, Hao Yu, Stefania Sciara, Benjamin Crockett, Ulf Peschel, Zhiming Wang, Rosario lo Franco, Mario Chemnitz, William J. Munro, David J. Moss, José Azaña, and Roberto Morandotti, “Progress in integrated and fiber optics for time-bin based quantum information processing”, Advanced Optical Technologies **14** 1560084 (2025). DOI 10.3389/aot.2025.1560084
186. Hao Yu, Benjamin Crockett, Nicola Montaut, Stefania Sciara, Mario Chemnitz, Sai T Chu, Brent E Little, David J Moss, Zhiming Wang, José Azaña, And Roberto Morandotti, “Exploiting nonlocal correlations for dispersion-resilient quantum communications”, ***Physical Review Letters*** **134** (2025).
187. Stefania Sciara, Piotr Roztocki, Bennet Fisher, Christian Reimer, Luis Romero Cortez, William J. Munro, David J. Moss, Alfonso C. Cino, Lucia Caspani, Michael Kues, J. Azana, and Roberto Morandotti, “Scalable and effective multilevel entangled photon states: A promising tool to boost quantum technologies”, Nanophotonics vol. 10 (18), 4447–4465 (2021). DOI:10.1515/nanoph-2021-0510.
188. L. Caspani, C. Reimer, M. Kues, et al., “Multifrequency sources of quantum correlated photon pairs on-chip: a path toward integrated Quantum Frequency Combs,” Nanophotonics, vol. 5, no. 2, pp. 351-362, 2016.
189. H. Yu, S. Sciara, M. Chemnitz, N. Montaut, B. Fischer, R. Helsten, B. Crockett, B. Wetzel, T. A. Göbel, R. Krämer, B. E. Little, S. T. Chu, D. J. Moss, S. Nolte, W.J. Munro, Z. Wang, J. Azaña, R. Morandotti, “Quantum key distribution implemented with d-level time-bin entangled photons”, ***Nature Communications*** **16** 171 (2025). DOI:10.1038/s41467-024-55345-0.